



Cytotoxic effects of engineered nanoparticles at the bio-nano interface

Presenter: Dr. Wen Zhang

PI: Dr. Yongsheng Chen

yongsheng.chen@ce.gatech.edu

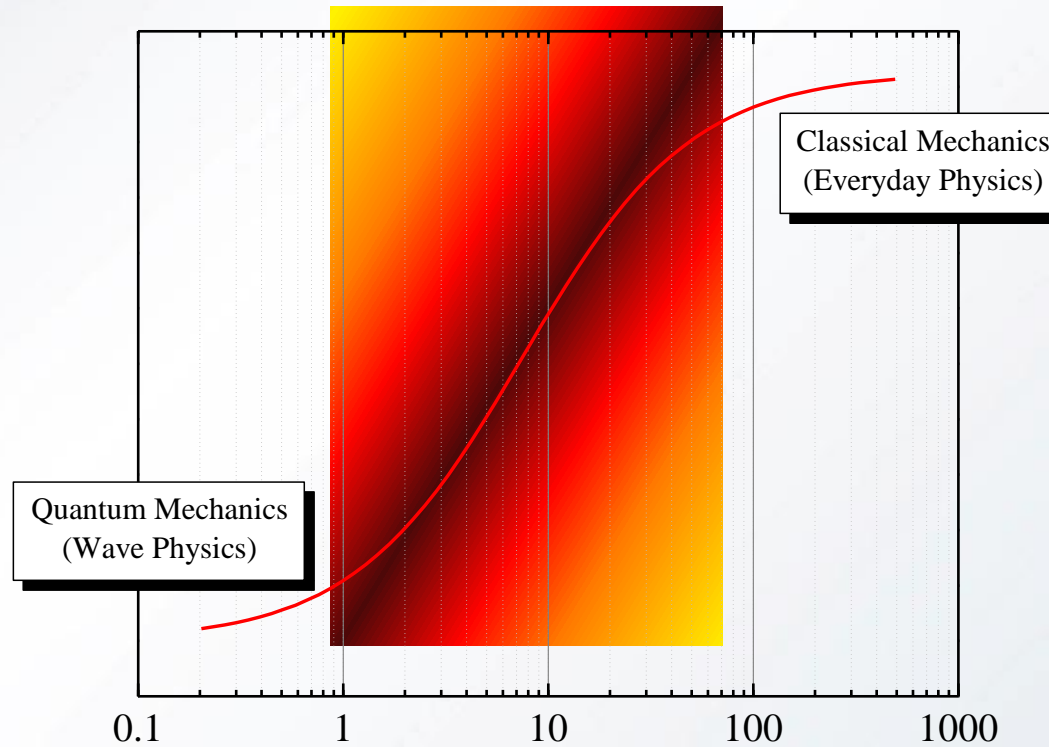
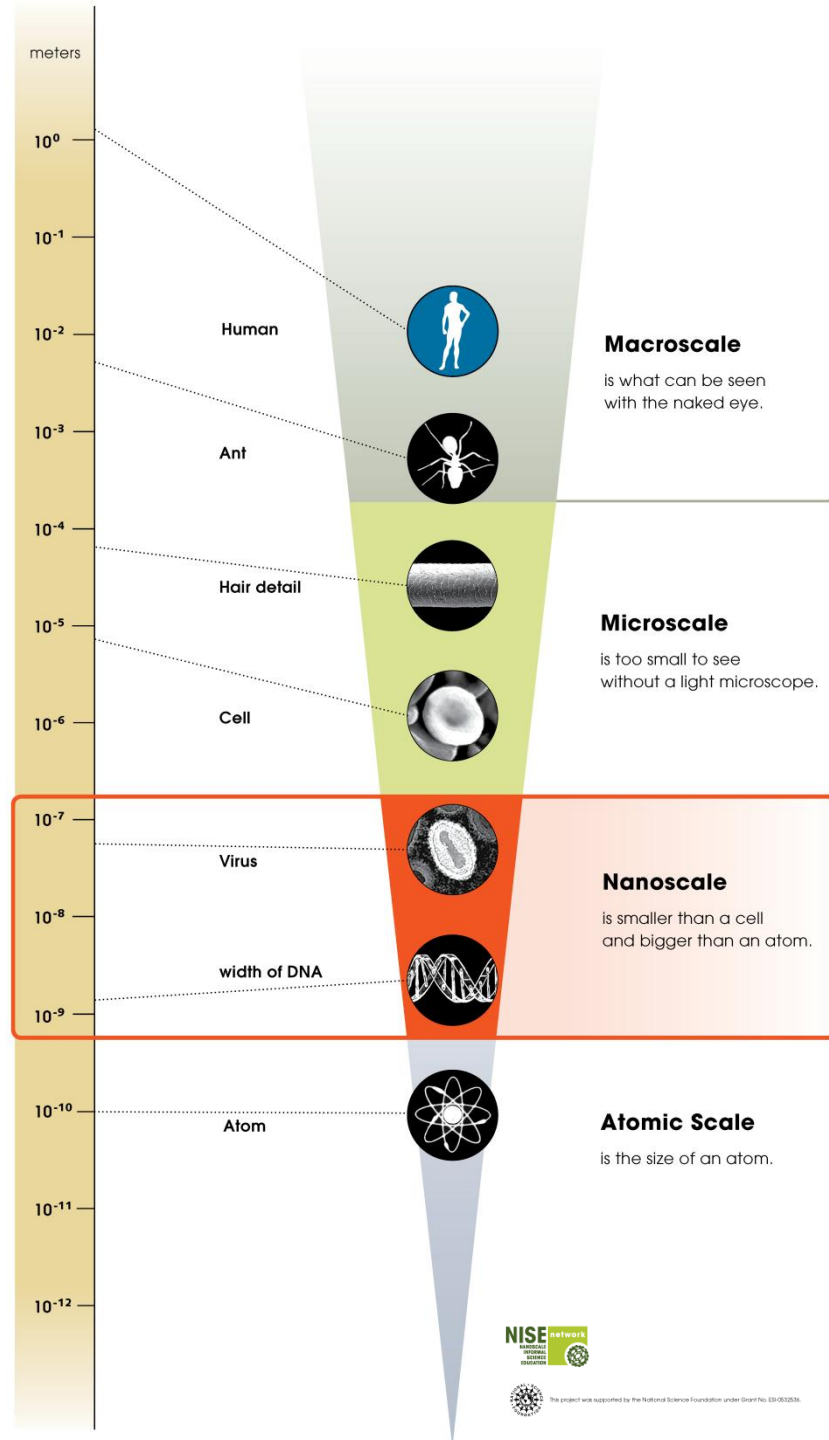
November 3 2011



**Georgia Institute
of Technology®**

School of Civil and Environmental Engineering

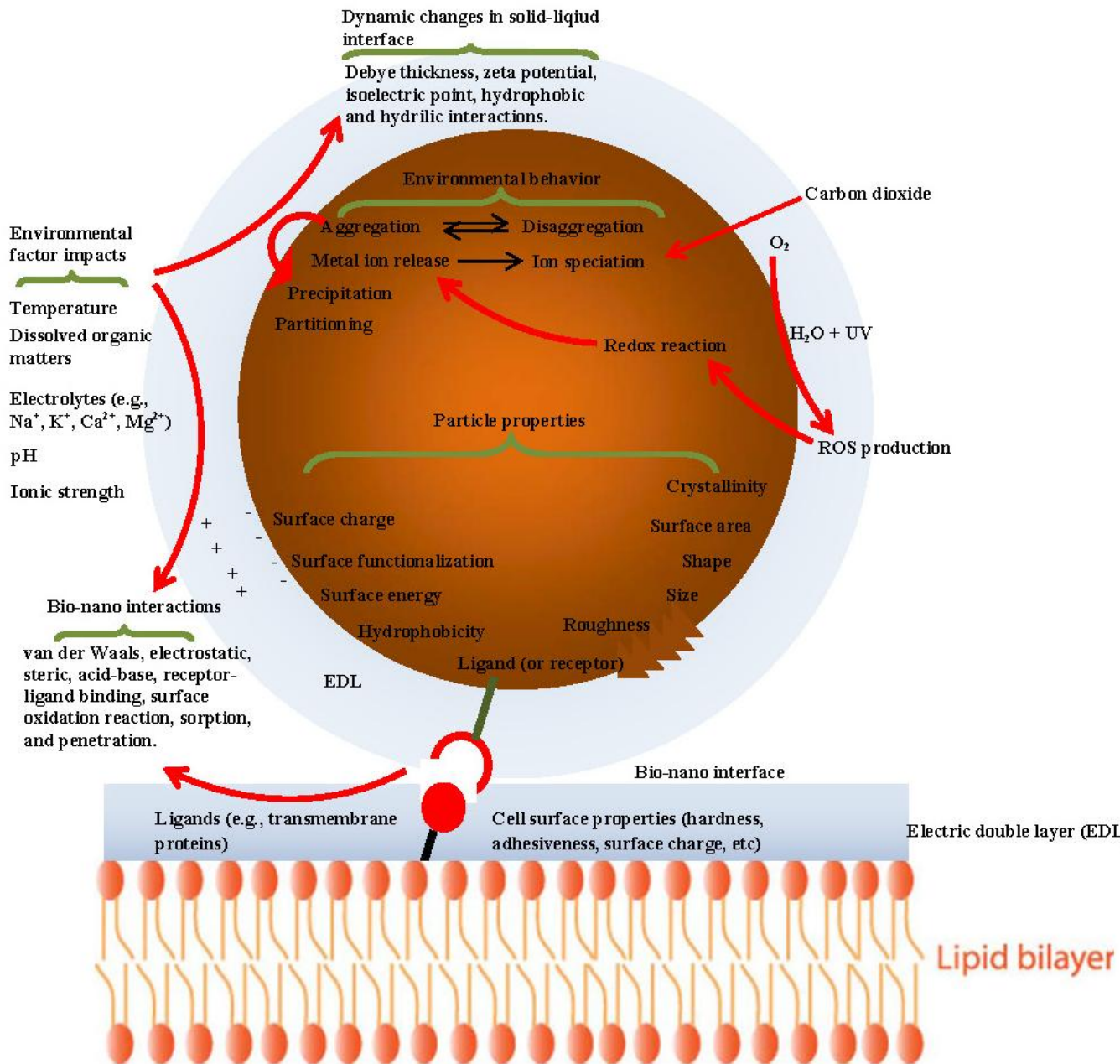
What happens at nanoscale?



- High specific surface area
- High reactivity
- High transportability
- More.....

What could

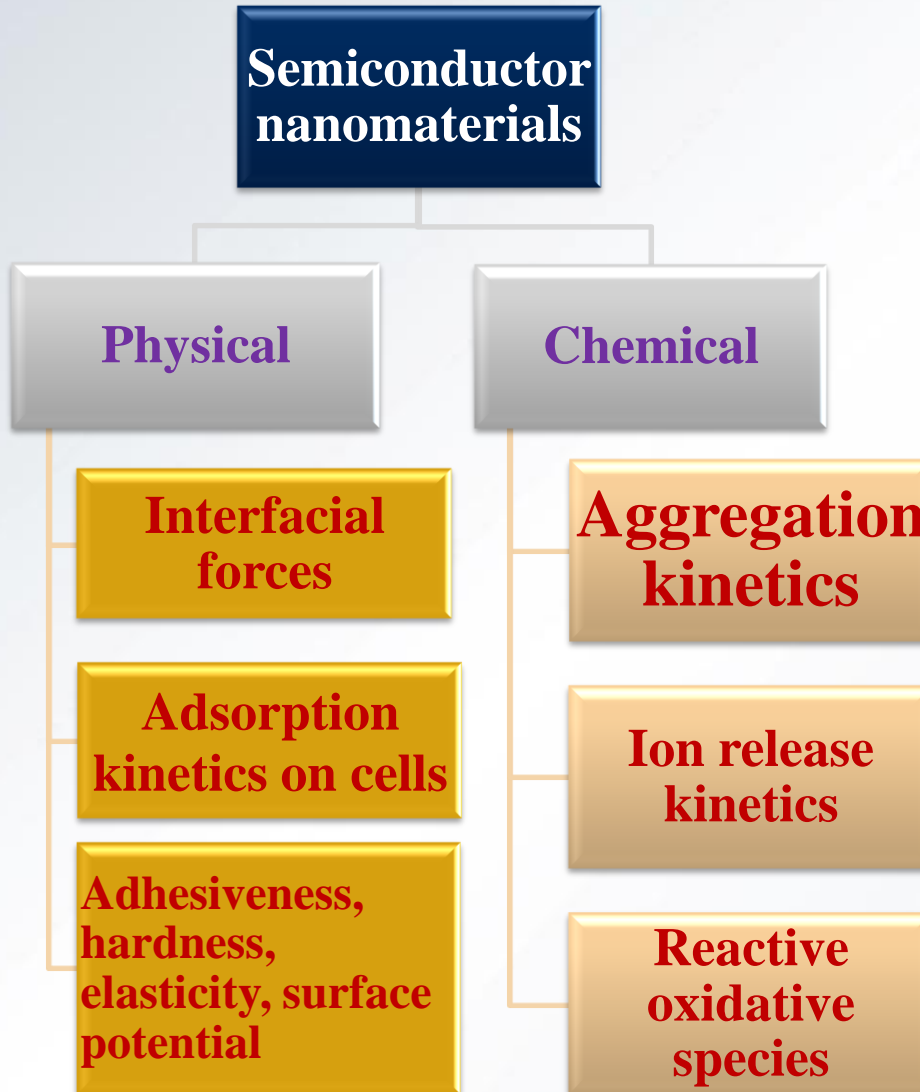
happen to NPs at biological interface?



- Adsorption
- Specific (ligand/receptor) and non-specific interactions
- Disruption (e.g., physical and chemical damage)
- Permeation/penetration

Figure 1.1. Representation of the interface between a nanoparticle and an intact lipid bilayer representative of a cell surface. Various environmental factors, particle properties, and their interrelationships are depicted. Credit: Wen Zhang. PhD thesis, Georgia Tech. 2011

My research outline



Fe_2O_3
CeO_2
TiO_2
ZnO
Al_2O_3
CuO
SiO_2
QDs
Au
Ag

Some of the key findings on adsorption kinetics and the associated cellular impairments

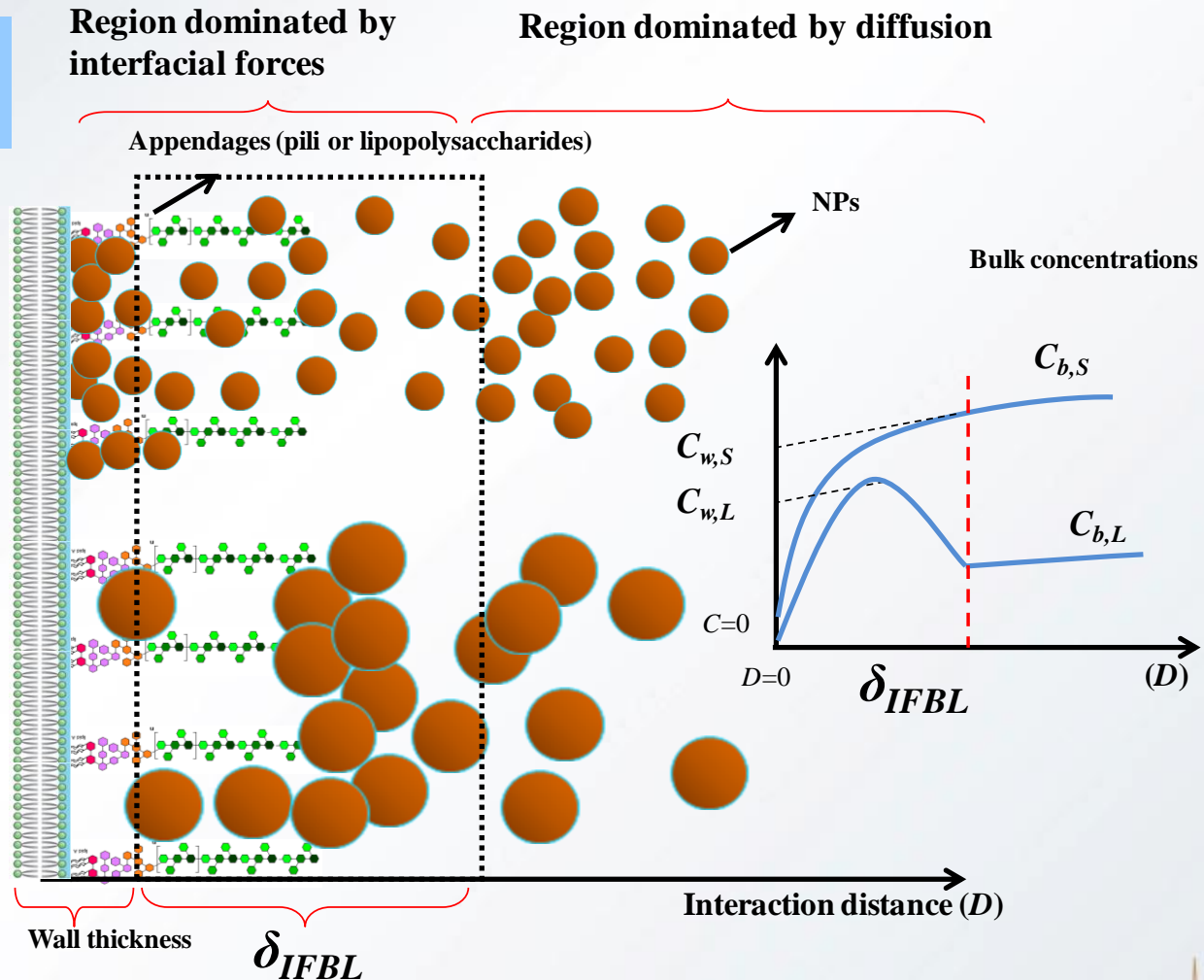
Interaction force boundary layer (IFBL) model



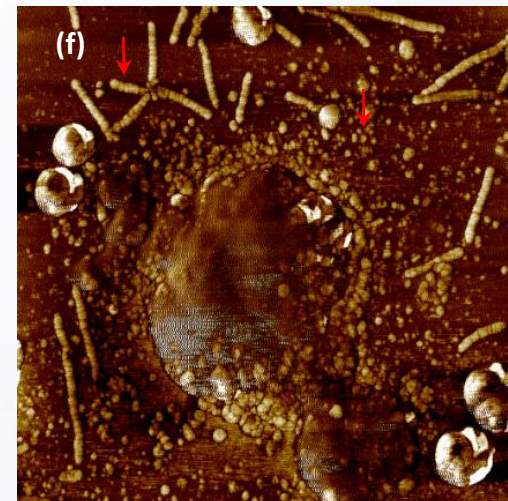
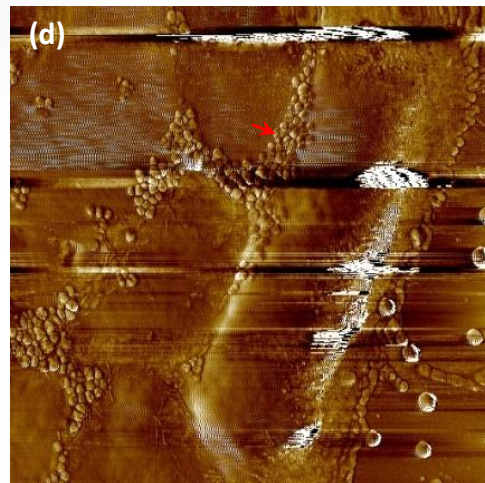
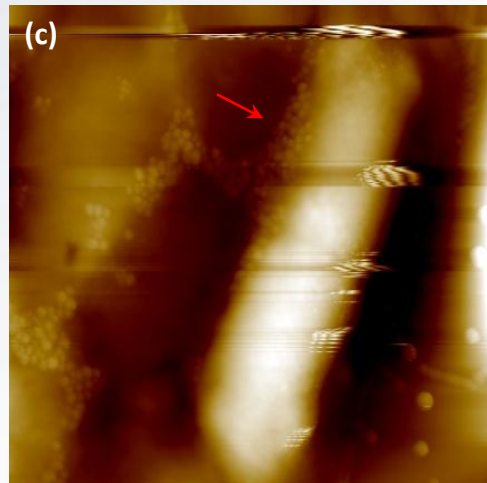
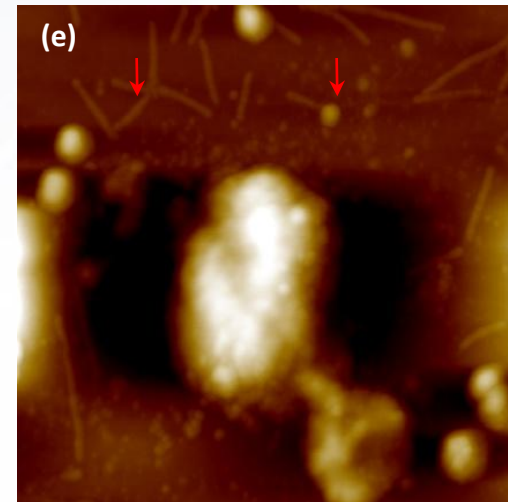
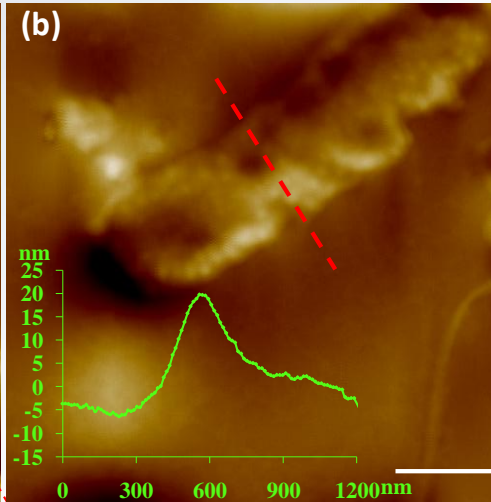
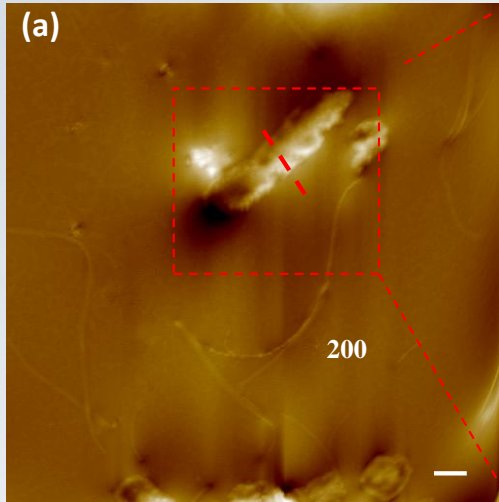
Role of random kinetic energy (diffusivity)

Role of interfacial energy

Adsorption kinetics (i.e., rate constant)

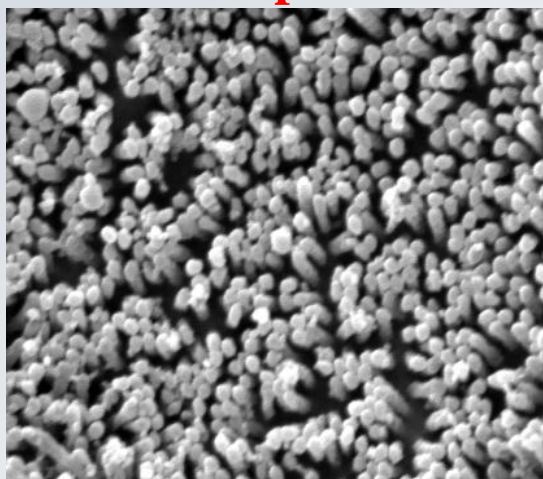


Surface disruption to bacteria (*E. coli*) after exposure to hematite NPs

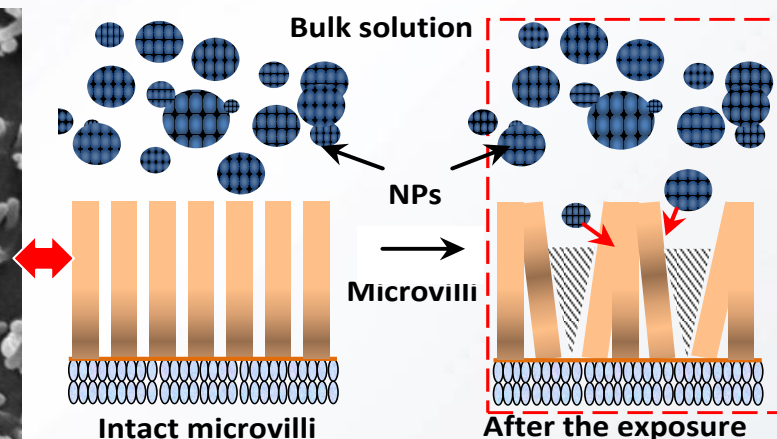
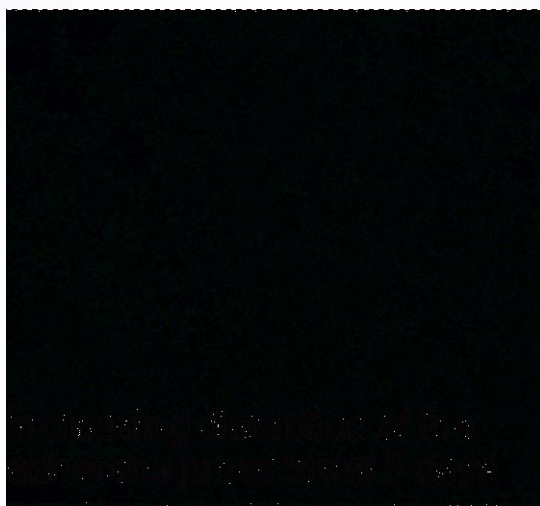
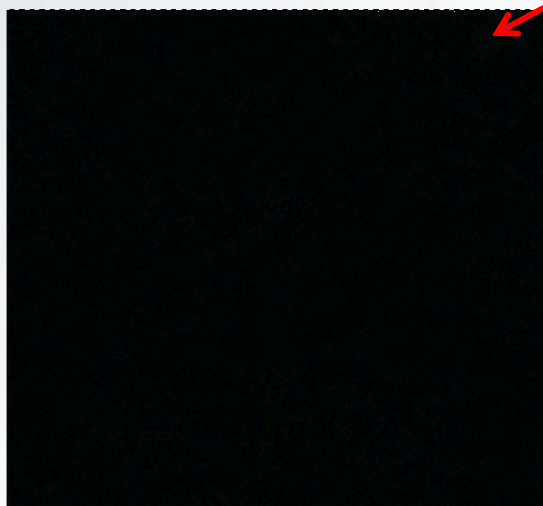
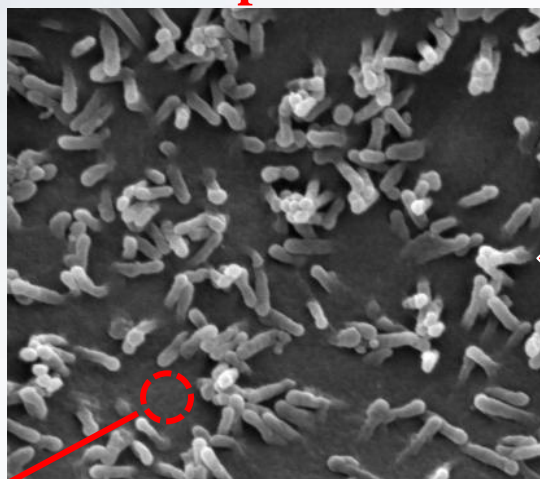


Surface disruption to human intestinal cells (Caco-2) after exposure to hematite NPs

Before exposure



After exposure

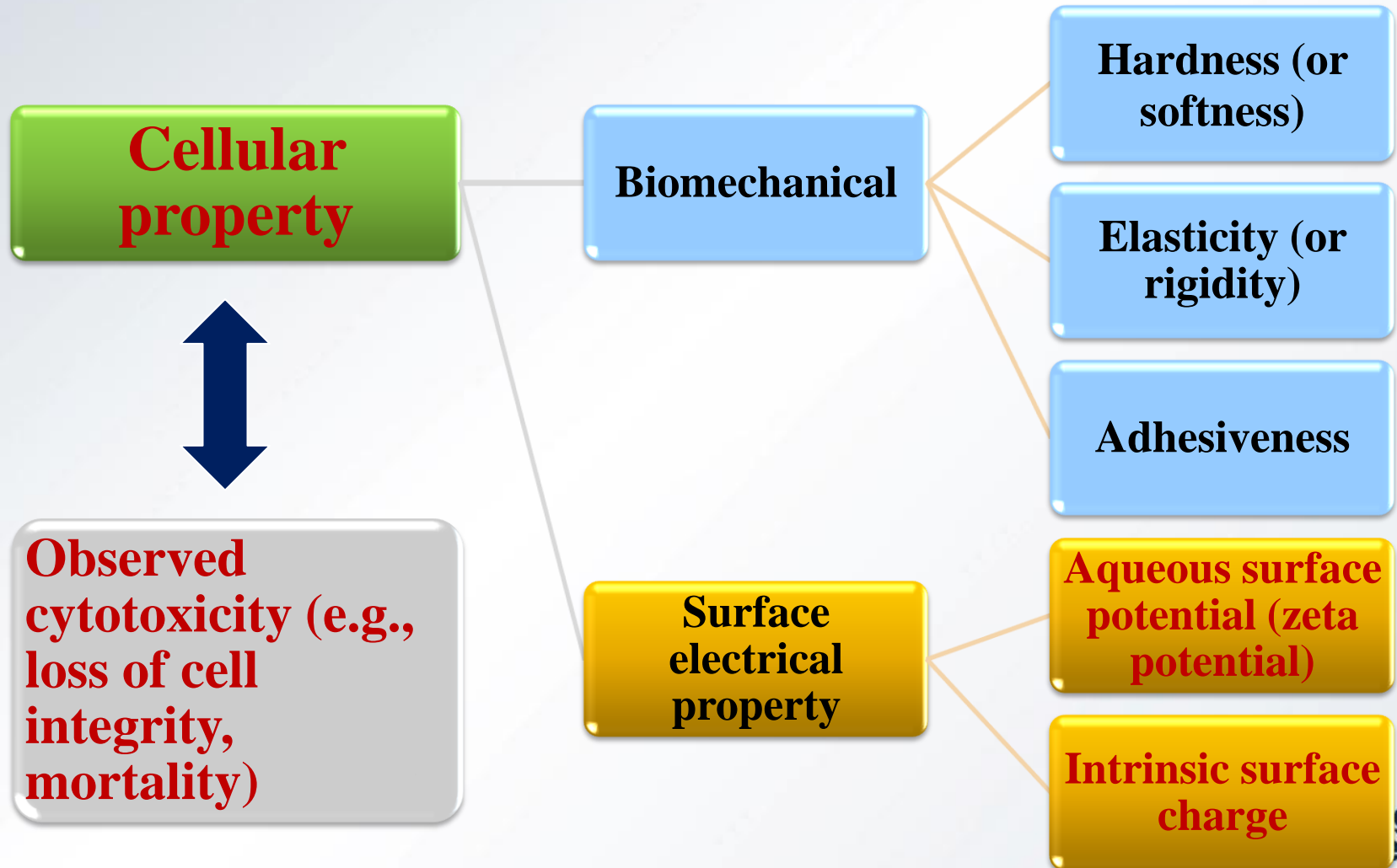


- Microvilli disruption, membrane penetration, and adheren junction disruption.
- Possibly interpreted by depletion attraction.

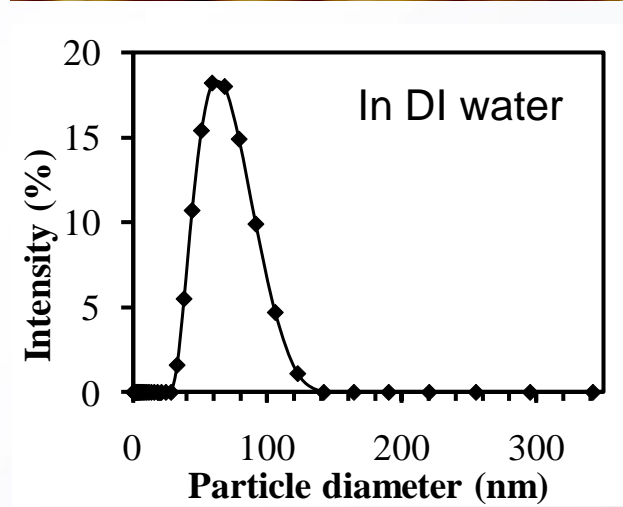
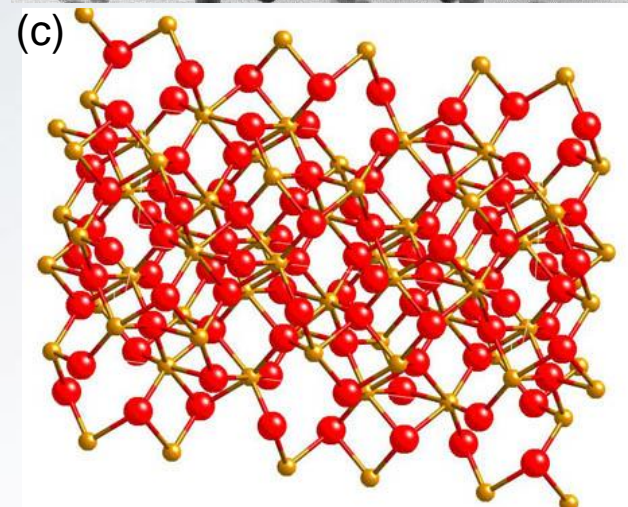
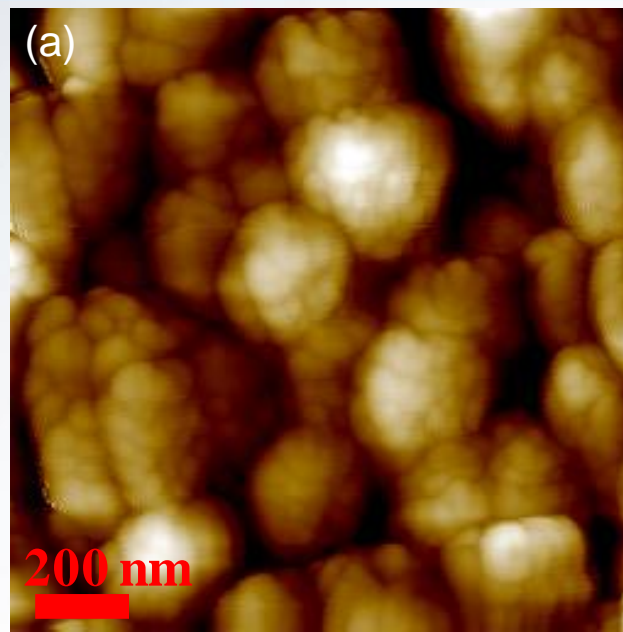
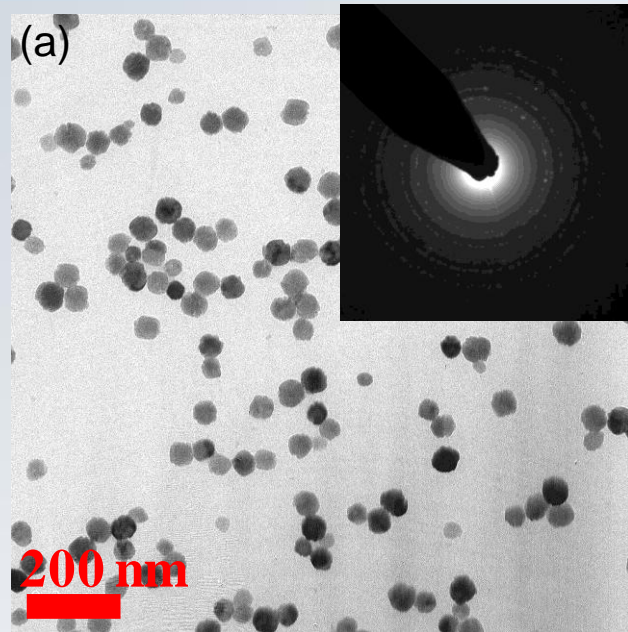
Wen Zhang, Madhavi Kalive, David G Capco, and Yongsheng Chen, Adsorption of hematite nanoparticles onto Caco-2 cells and the cellular impairments: effect of particle size. *Nanotechnology* 2010, 21, 355103.

Mechanisms of surface disruption from a physical perspective: Fe_2O_3 vs *E. coli*

To better understand and interpret nanotoxicity test results:



Mechanisms of surface disruption from a physical perspective: Fe_2O_3 vs *E. coli*



(a) TEM image of hematite ($\alpha\text{-Fe}_2\text{O}_3$) NPs with inset of SAED pattern; (b) AFM image of aggregated clusters of hematite NPs; (c) Crystal structure of hematite NPs; and (d) The size distribution

Several important features of hematite (reasons of choosing it in the test)

- ✓ Good reference nanomaterial
- ✓ Good aqueous stability
- ✓ Relatively uniform size distribution
- ✓ No toxic metal release (good chemical stability or chemically inert)

Mechanisms of surface disruption from a physical perspective: Fe_2O_3 vs *E. coli*



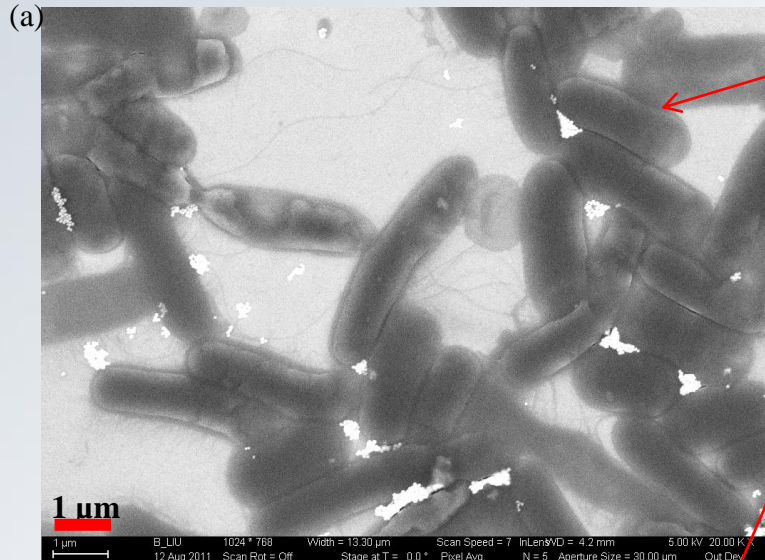
Reprehensive morphology of *E. coli* cells

Several important advantages by using *E. coli* as a cell target

- ✓ One of the basic and representative **Gram-negative** bacterial form that mirrors most of the bacterial properties
- ✓ Rapid toxicity screening relative to human cell lines
- ✓ A **representative microorganism** widely used in nanotoxicity tests
- ✓ Commonly used experimentally in **molecular biology**
- ✓ Comprehensive knowledge of gene library that allows us to conduct future genetic level studies

Results

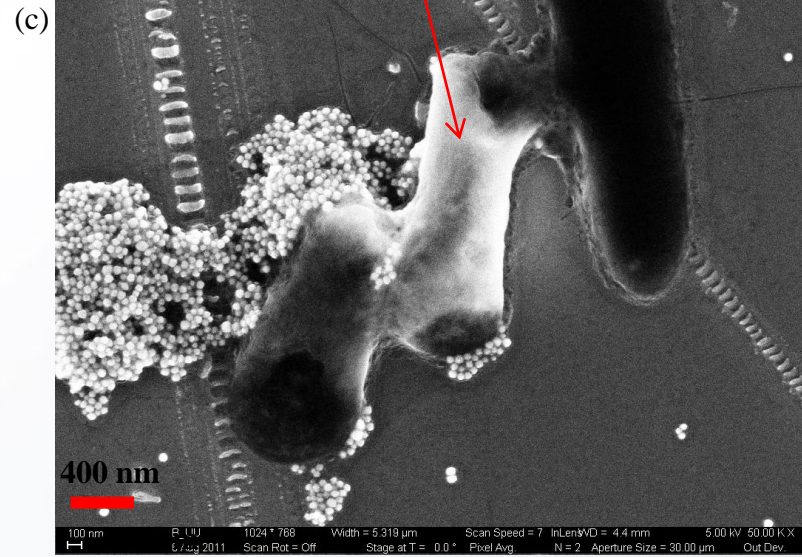
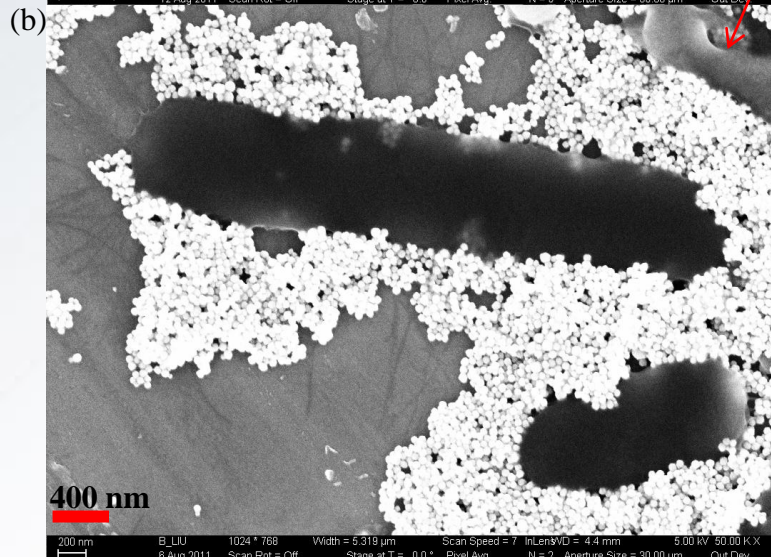
1. Morphology changes of *E. coli* after exposure to hematite NPs



E. coli cells with a few hematite NPs (white dots) attached

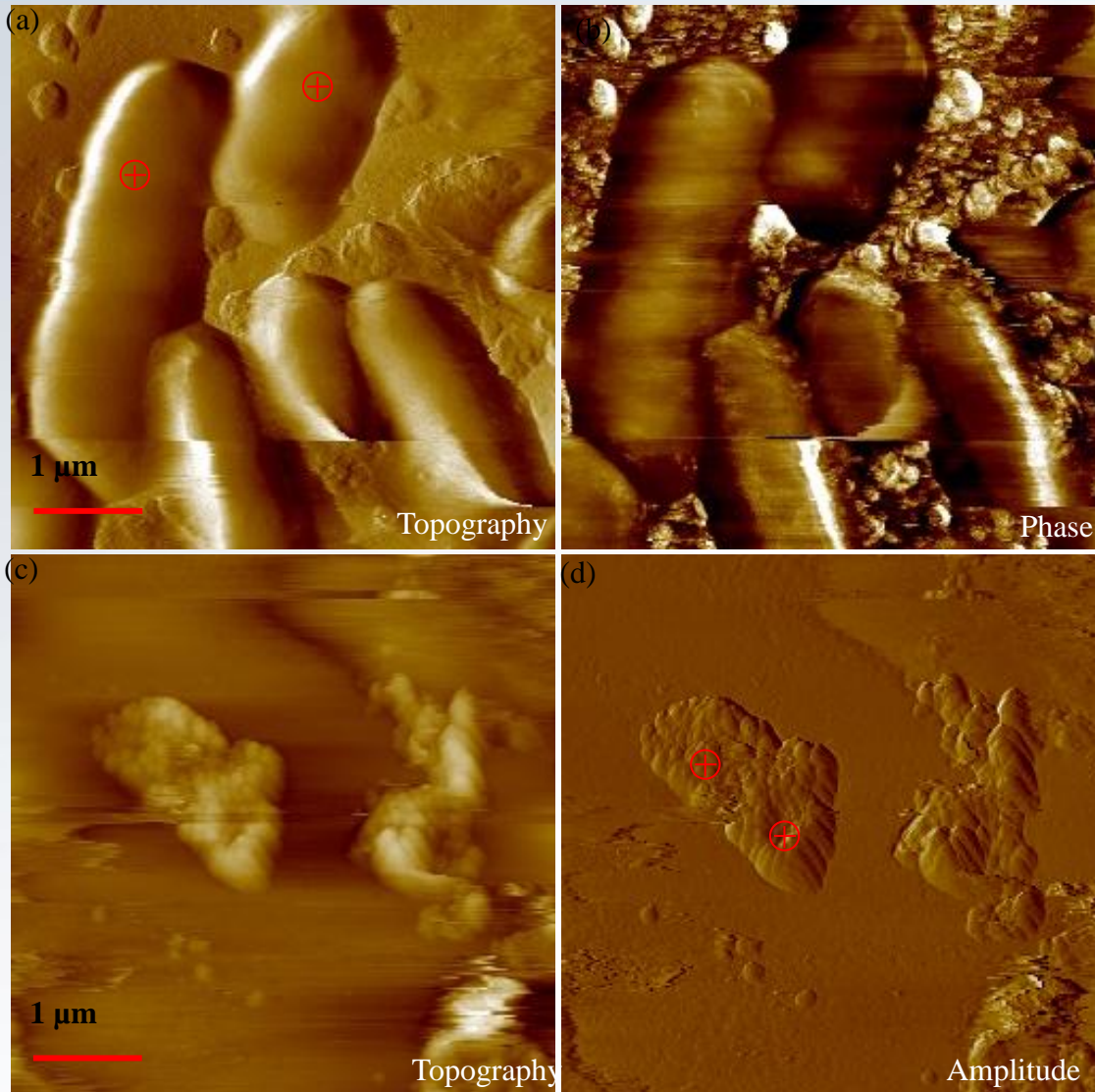
E. coli cells with heavy adsorption of hematite NPs and aggregated clusters

Deformed *E. coli* cells after long time exposure to hematite NPs



Results

1. Morphology changes of *E. coli* after exposure to hematite NPs



Quasi-in situ imaging of *E. coli* cells in liquid by AFM.

- ❖ *E. coli* cells immobilized on a freshly cleaned silicon wafer surface treated with poly-L-lysine

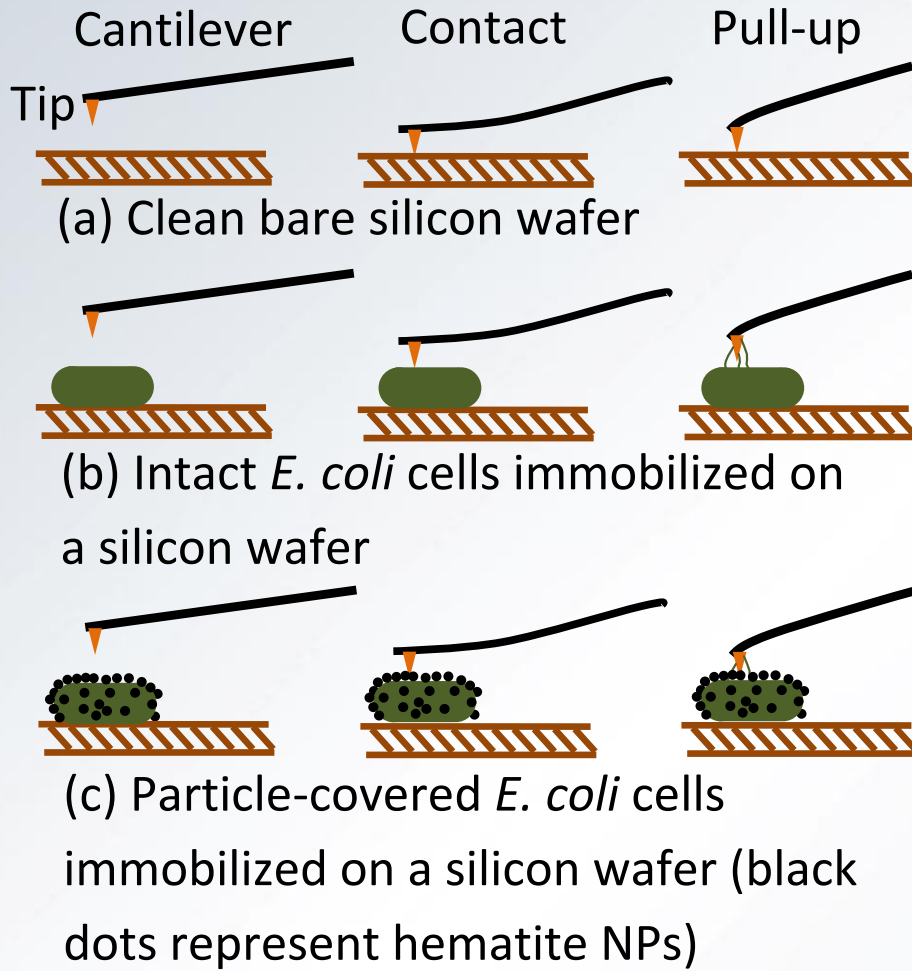
- ❖ *E. coli* cells maintained a hydrated appearance

- ❖ Smooth outer surface without surface ultrastructures or flagella resolved

- ❖ *E. coli* cells and that the bacterial cells shrunk significantly.

Results

2. Biomechanical property changes of *E. coli* cells at local scale



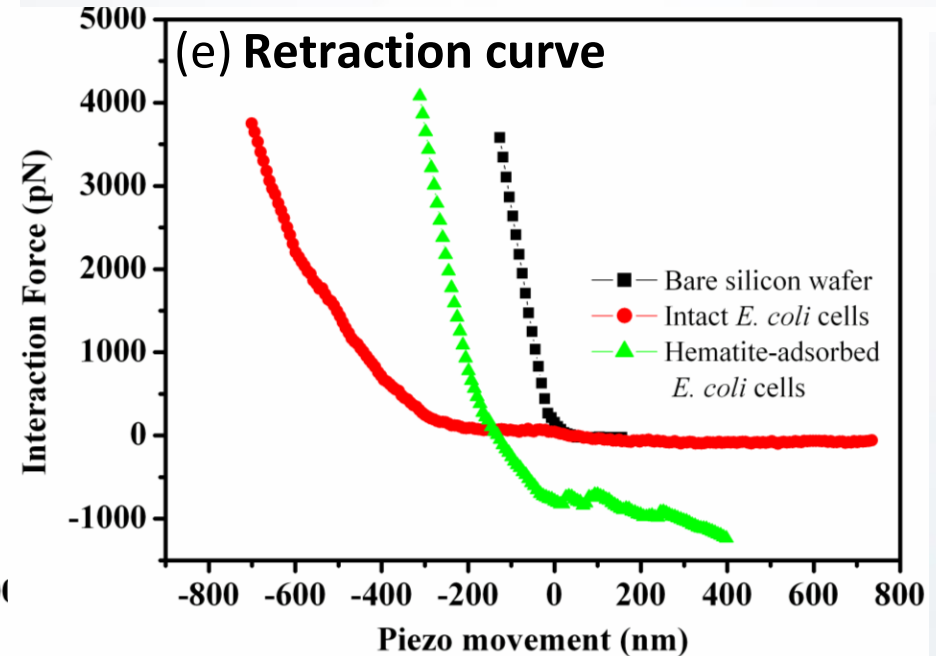
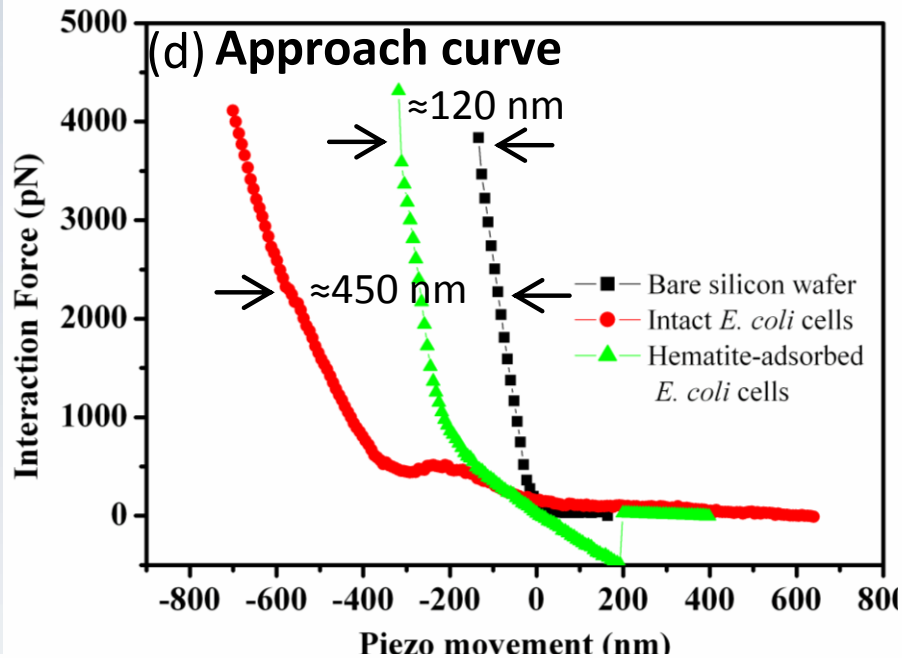
Force measurement by AFM.

- ❖ The resulting force-distance curves can be used to estimate surface hardness, elasticity, and adhesiveness.
- ❖ Hardness is indicated by the indentation of the tip engaged with the sample surface
- ❖ Elasticity is measured by spring constant of the cell
- ❖ Adhesiveness is directly reflected by the adhesion force between the tip and the cell surface

The illustrations are not drawn to scale.

Results

2. Biomechanical property changes of *E. coli* cells at local scale



Force-distance curves as the tip approached and retracted from the contact with sample surfaces at a maximum loading force of approximately 4 nN (averaged from 6-20 replicates).

- Intact *E. coli* cells had indentation 250–450 nm, which is dependent on accurate estimation of the contact point; impaired cells only had an average indentation of 120 nm.
- No adhesion on intact untreated cells, whereas large adhesion was detected on treated cells

Results

2. Biomechanical property changes of *E. coli* cells at local scale

The spring constant of the cell (k_b) can be calculated using the equation: $k_b = k_c s / (1 - s)$

where k_c is the spring constant of the cantilever and s is the slope in the linear compliant region of the force-distance curve.

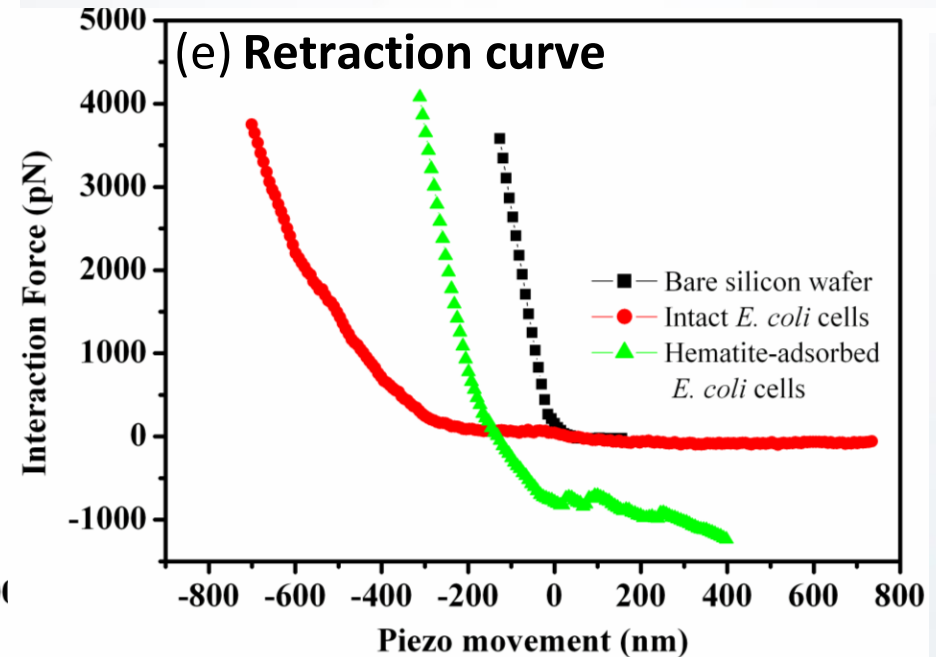
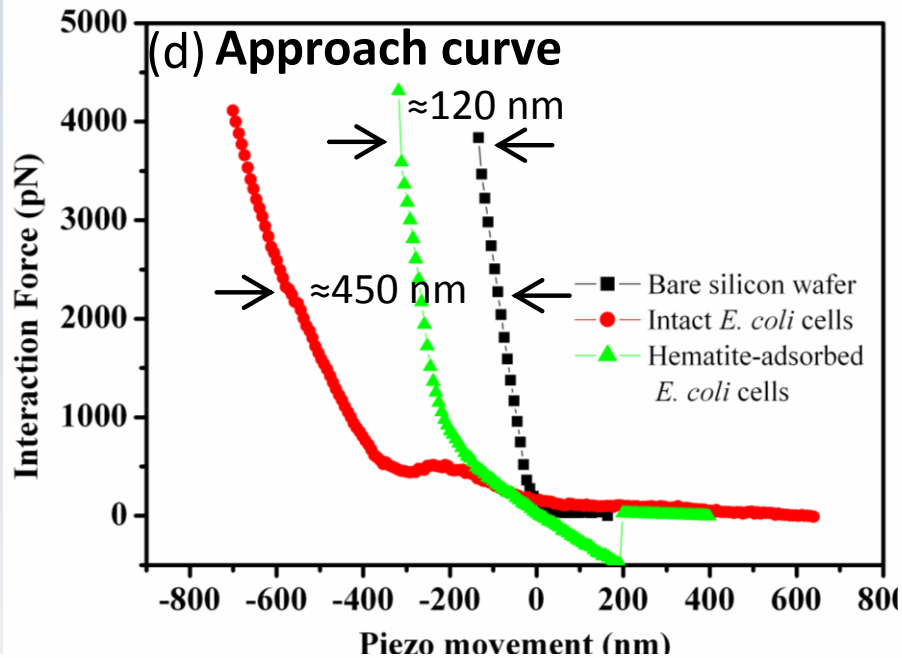
Table 1 Summary of spring constants for untreated and hematite-treated *E. coli* cells.

	Cantilever spring constant, k_c , (nN/nm)	Slope (nm/nm)*	Spring constant of the cells, k_b , (nN/nm)
Untreated <i>E. coli</i> cells	0.03±0.01	0.307 ± 0.02	0.013
Hematite-treated <i>E. coli</i> cells		0.904 ± 0.02	0.283 → Less elastic

*The slope (nm/nm) was converted from the slope (nN/nm) in the force-distance curve dividing by the spring constant of the cantilever.

Results

2. Biomechanical property changes of *E. coli* cells at local scale



Force-distance curves as the tip approached and retracted from the contact with sample surfaces at a maximum loading force of approximately 4 nN (averaged from 6-20 replicates).

➤ Intact *E. coli* cells had indentation 250–450 nm, which is dependent on accurate estimation of the contact point; impaired cells only had an average indentation of 120 nm.

➤ No adhesion on intact untreated cells, whereas large adhesion was detected on treated cells

Results

3. Zeta potential and electrical double layer (EDL) theory

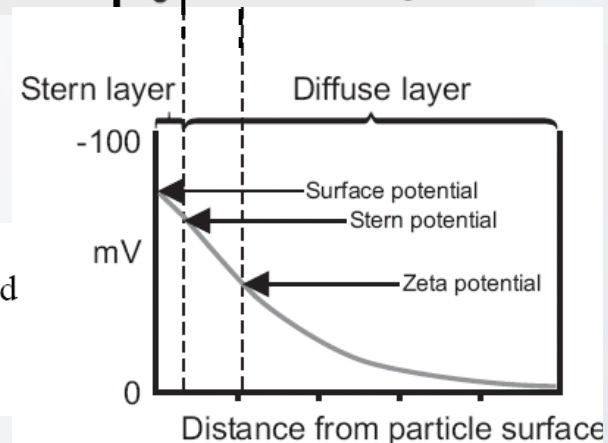
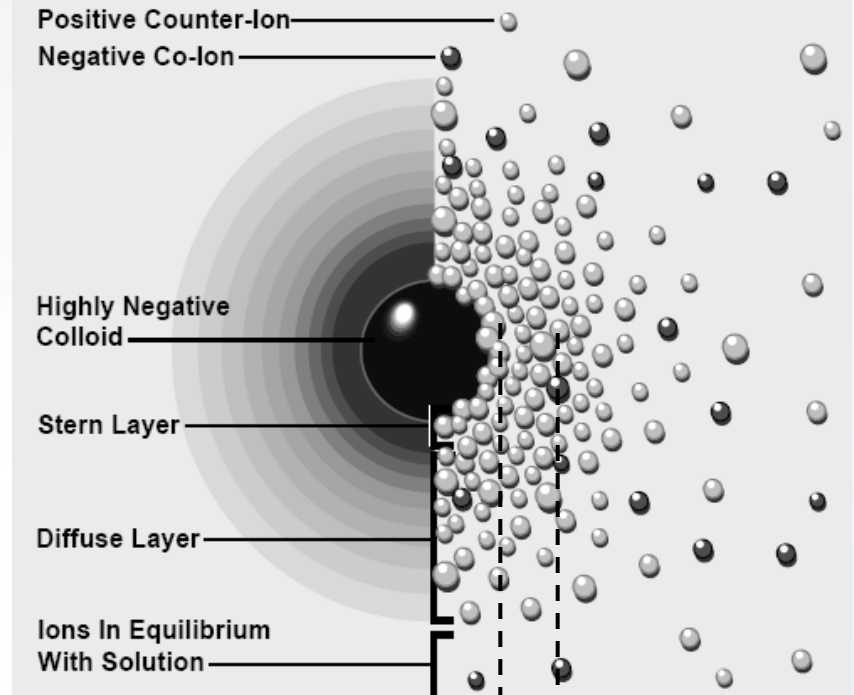
E. coli cells, when suspended in liquid, are subject to hydration and forming a EDL. The overall electrical property can be described by zeta potential.

Zeta potential (ζ) is commonly in aquatic chemistry and is measured by **Laser Doppler electrophoresis**.

The **electrophoretic mobility (μ_E)** is directly measured and ζ potential is converted from **Henry's approximation**:

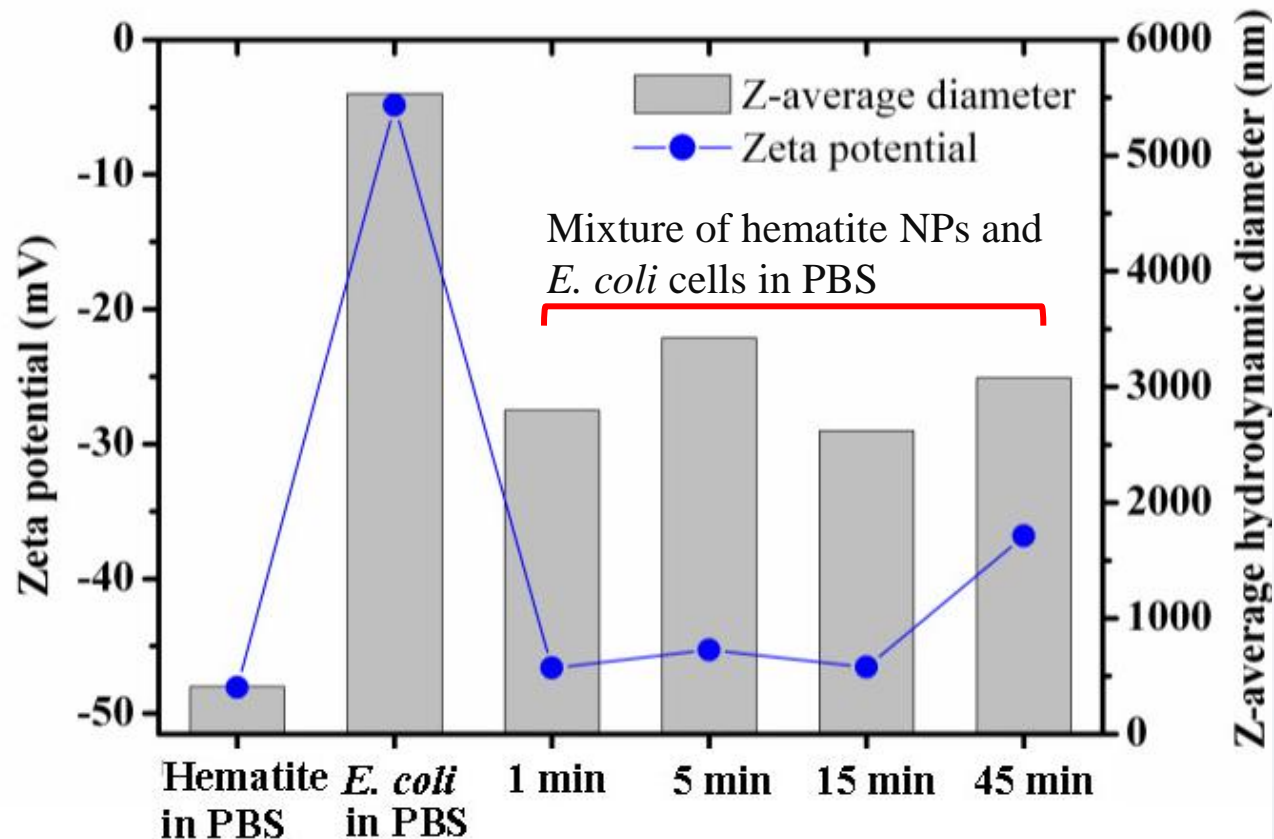
$$\mu_E = \frac{2\zeta\epsilon f(\kappa r)}{3\eta}$$

where ϵ is the dielectric constant (or permittivity); η is the medium's viscosity (i.e., the viscosity of water); κr is the ratio of particle radius to Debye double layer thickness; and $f(\kappa r)$ refers to Henry's function, which is 1.5 under the Smoluchowski approximation and 1 under the Hückel approximation.



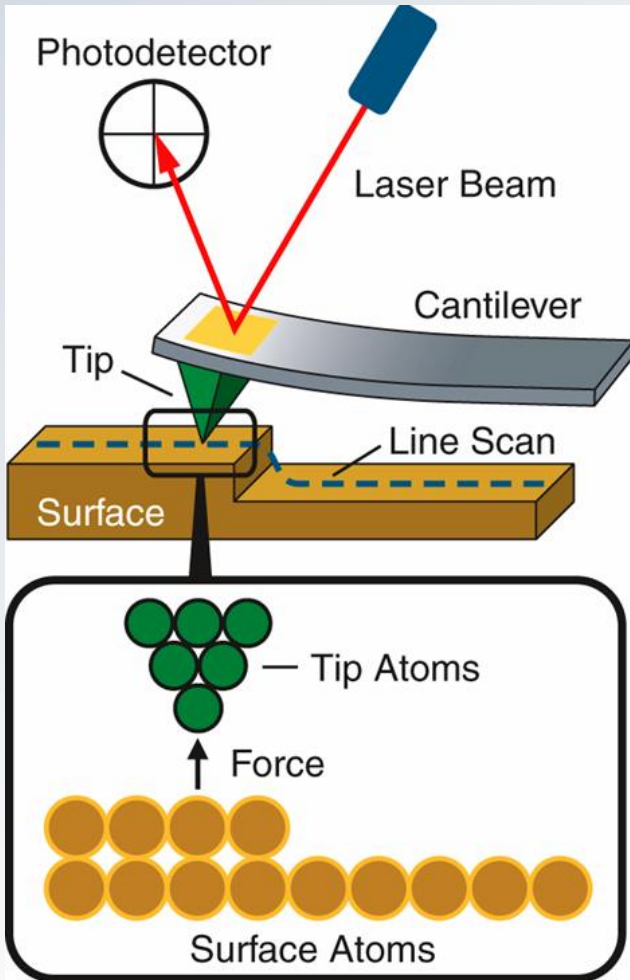
Results

3. Zeta potential and electrical double layer (EDL) theory



Results

4. Surface electric potential probed by KPFM



Schematic of AFM

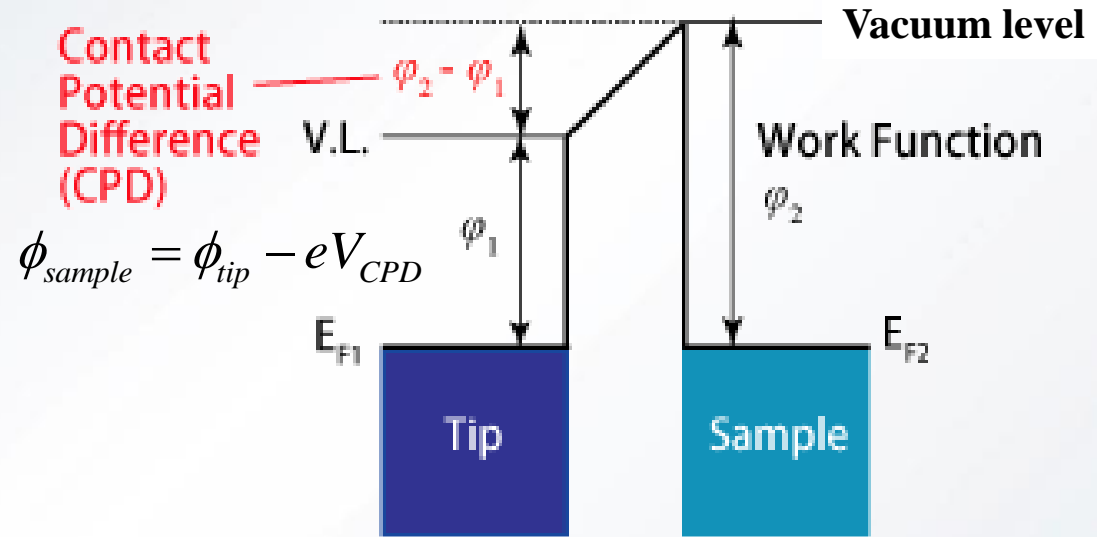
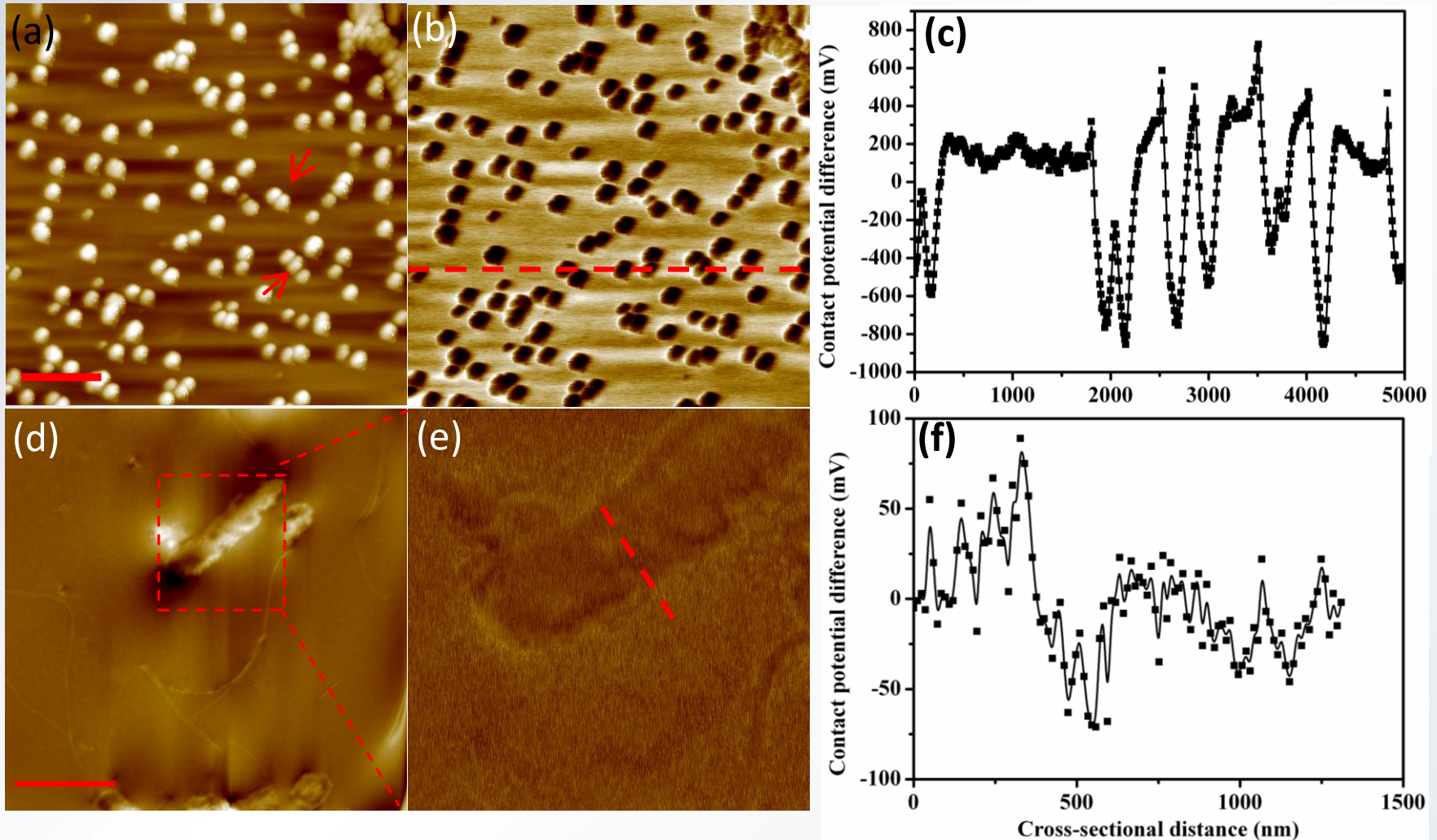


Fig. 2. Band diagram of tip and sample according to the operation principle of KPFM

In metals, CPD can be the energy difference between the vacuum level and the Fermi energy.
In semiconductors or biomolecules, the work function may arise from the difference in energy between the vacuum level and the most loosely bound electron inside the sample.

Results

4. Surface electric potential probed by KPFM



Topographical and surface potential images of hematite NPs and intact *E. coli* cells generated by KPFM. (a) and (d) are topographical images. (b) and (e) are surface potential images. (c) and (f) are cross-sectional profiles of surface potentials taken along the dashed red lines in the images in (b) and (e). The red solid lines at the bottom right in (a) and (d) indicate scale bars of 0.5 and 1 μm, respectively.

Results

4. Surface electric potential probed by KPFM

- The relation between the work function of the conductive tip, Φ_t , and the sample, Φ_s , is given by $\Phi_s = \Phi_t - eV_{CPD}$, where e is the elementary charge and V_{CPD} is the CPD or surface potential measured by KPFM. Thus, the mean work function of hematite NPs is approximately **5.71 eV**.
- Literature reported value of the work function or Fermi level is **5.88 eV** and the minor difference is probably due to the moisture on hematite surface that induced band bending.

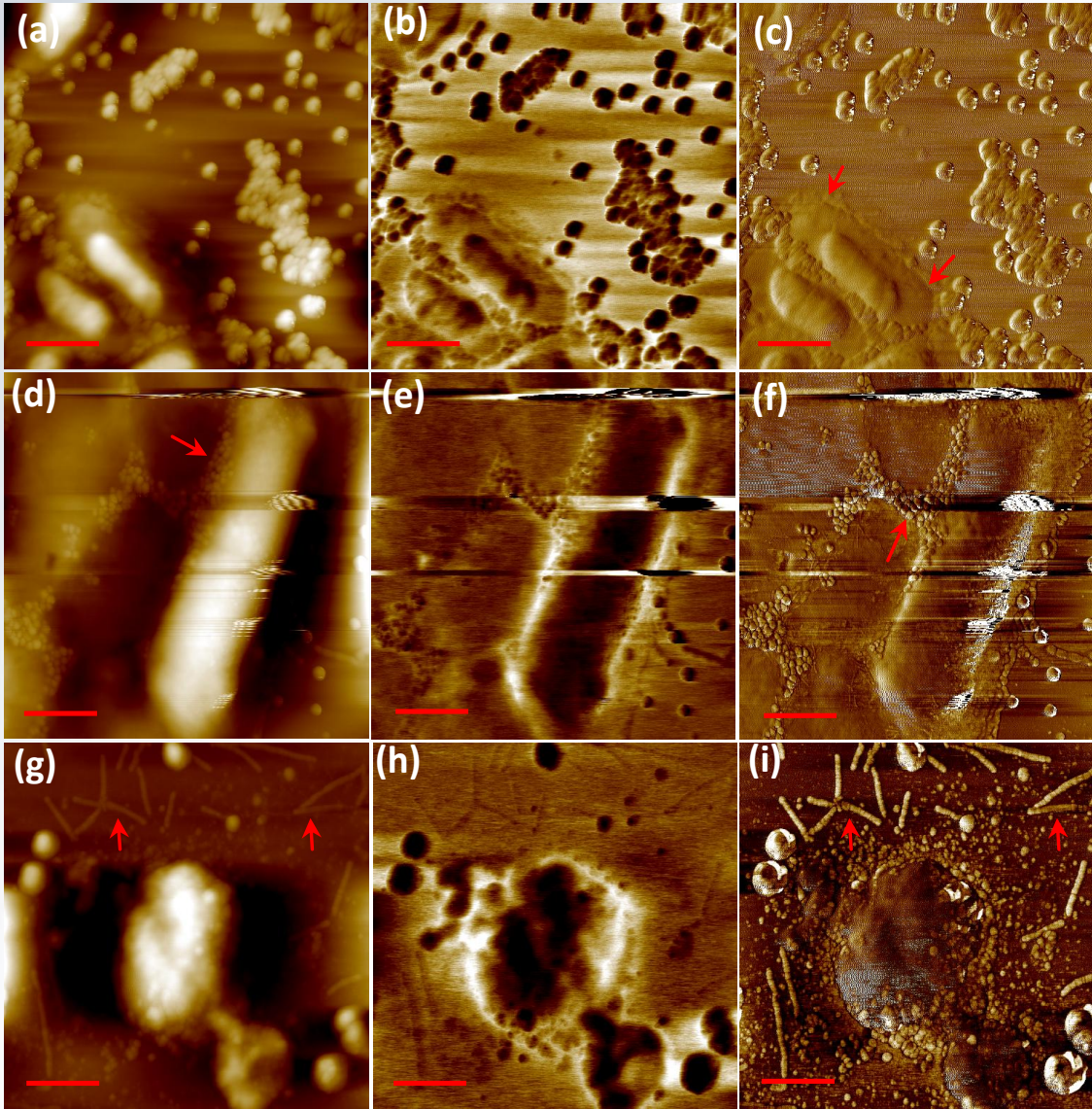
Results

4. Surface electric potential probed by KPFM

Topography

Surface Potential

Phase



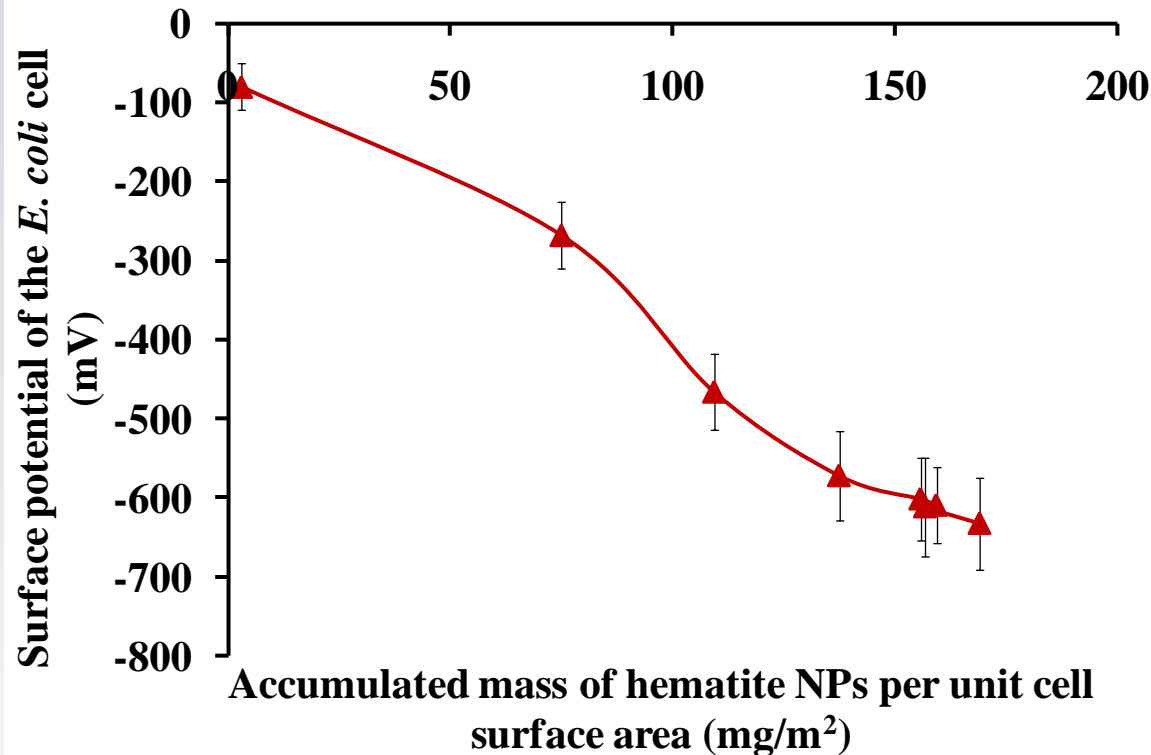
The topographical (left column), surface potential (middle column), and phase (right column) images of *E. coli* cells exposed to hematite NPs (98 nm). Exposure times were approximately (a)-(c) 3 min; (d)-(f) 10 min; and (g)-(i) 45 min. The red scale bars at the bottom right of (a)-(c) and (d)-(i) indicate lengths of 2 μm and 0.5 μm, respectively.

- Deformation observed with hematite NPs adsorbed and the increasing adsorption time
- Surface appendage (flagella) shredded and scattered around.

Wen Zhang, Joseph B Hughes, and Yongsheng Chen. Impacts of hematite nanoparticle exposure on biomechanical and surface electrical properties of *E. coli* cells. *Applied Environmental Microbiology*, Submitted.

Results

4. Surface electric potential probed by KPFM



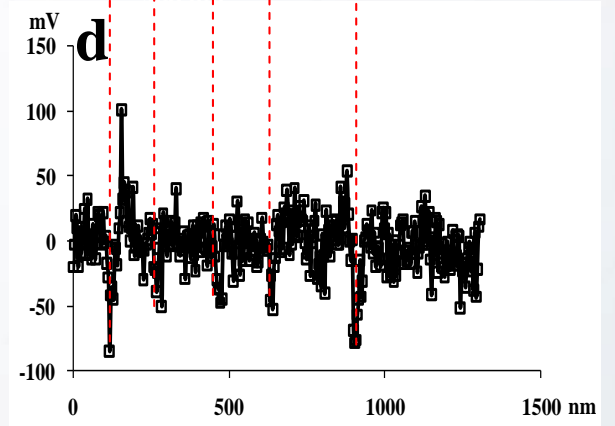
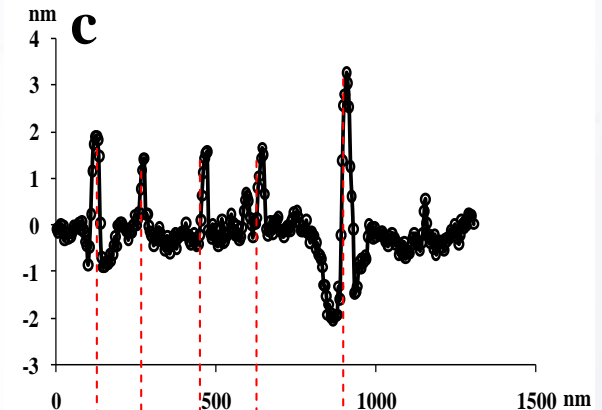
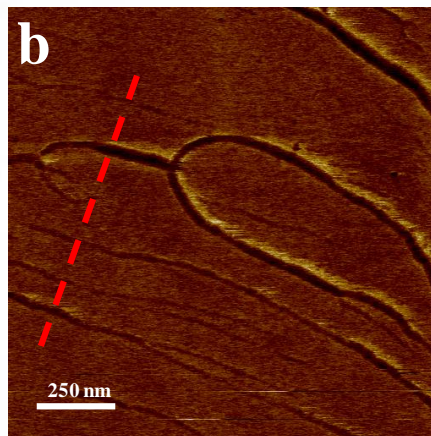
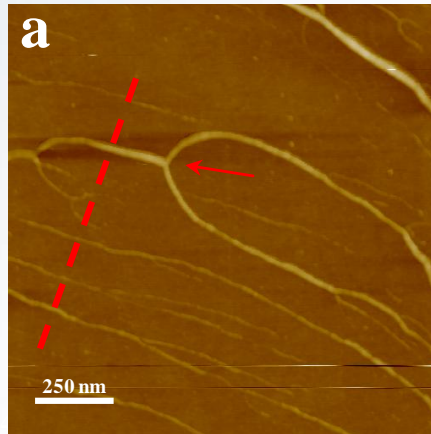
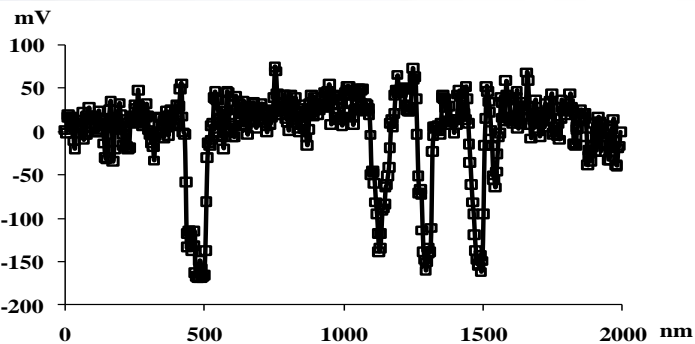
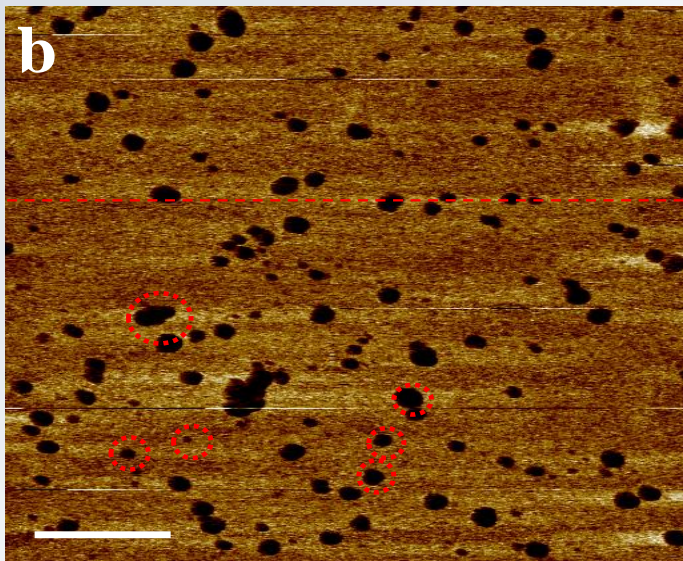
- ❑ Similar to the finding of zeta potentials but.....
- ❑ Quite different in the meaning of the electric potential
- ❑ Visualization of surface heterogeneities
- ❑ Local surface potential down to the resolution of the cantilever tip diameter

Surface became more negatively charged as more hematite attached.

Results

4. Surface electric potential probed by KPFM

My previous work on basis of KPFM focused on differentiation of interacting entities (DNA and QDs) at nanoscale.

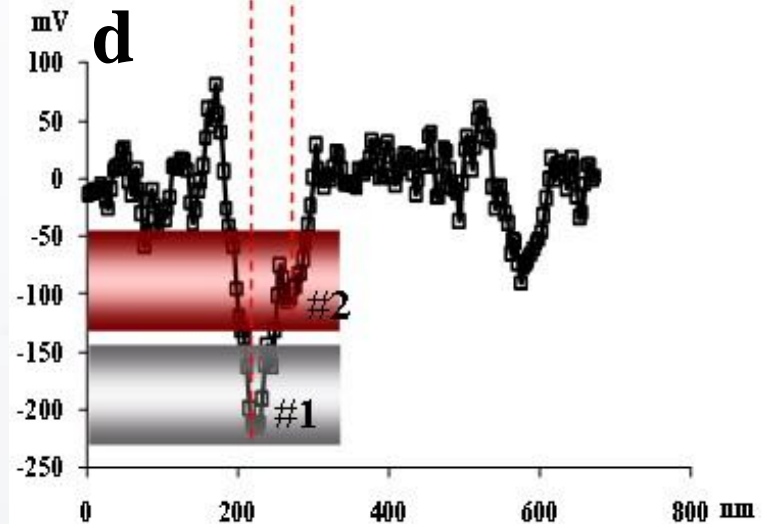
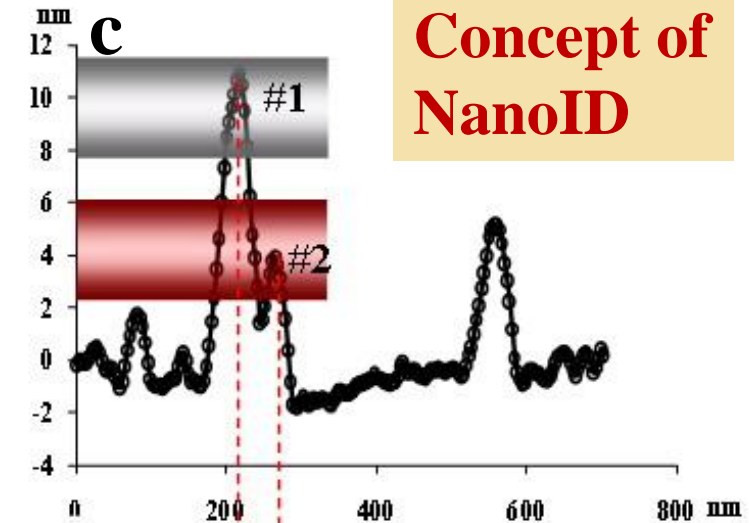
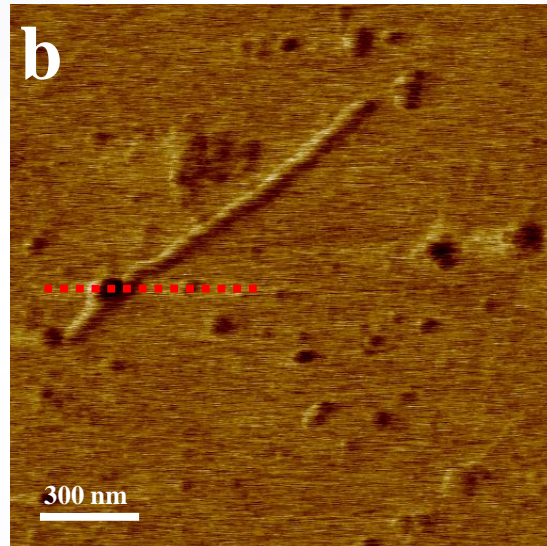
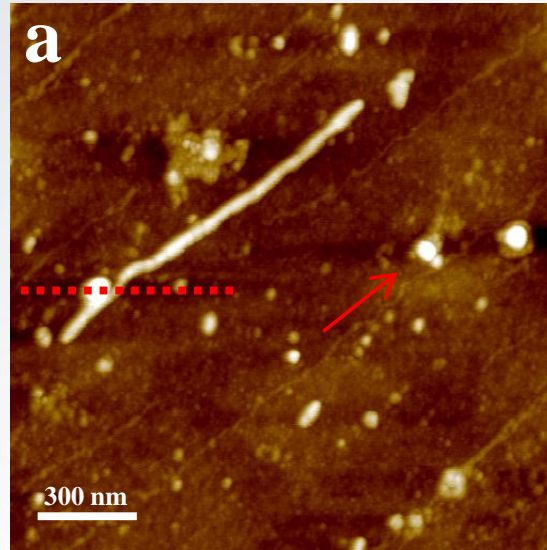


Wen Zhang, Ying Yao, and Yongsheng Chen Quantifying and Imaging the Morphology and Nanoelectric Properties of Soluble Quantum Dot Nanoparticles Interacting with DNA. *Journal of Physical Chemistry C*, 2011, 115 (3), 599-606.

Results

4. Surface electric potential probed by KPFM

The **topography** and **surface potential** differences enable us to better differentiate and quantify QDs bound with DNA.



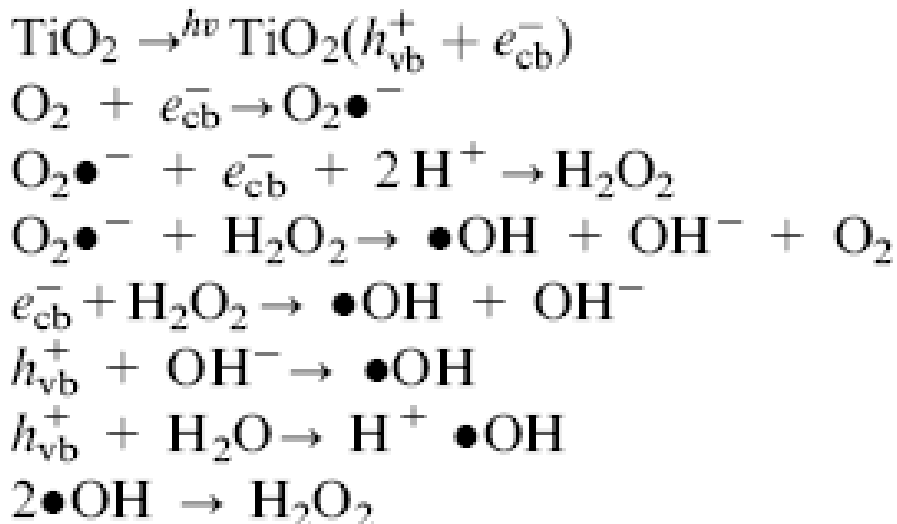
Wen Zhang, Ying Yao, and Yongsheng Chen Quantifying and Imaging the Morphology and Nanoelectric Properties of Soluble Quantum Dot Nanoparticles Interacting with DNA. *Journal of Physical Chemistry C*, 2011, 115 (3), 599-606.

Brief conclusion

- The *E. coli* cell surface became coarser, stiffer, and more adhesive with hematite NPs attached.
- Surface potential shifted to more negatively charged with the attachment of hematite NPs, observed by both zeta potential and KPFM.

Mechanisms of surface disruption from a chemical perspective

- High surface area of NPs provides more reactive sites for ROS production
- ROS formed in NP suspension usually consist of **superoxide radical ($O_2^{\bullet-}$)**, **hydroxyl radicals ($\bullet OH$)**, and **singlet oxygen (1O_2)**
- Representative reaction stoichiometry (TiO_2 as an example):



Implications:

- **Dissolution of metal ions (potentially hazardous to cells);**
- **Oxidant injury of cells, lipid peroxidation, enzyme or protein oxidation, membrane pitting, changes in membrane permeability, etc.**

Almost all types of engineered NPs were reported to produce ROS!

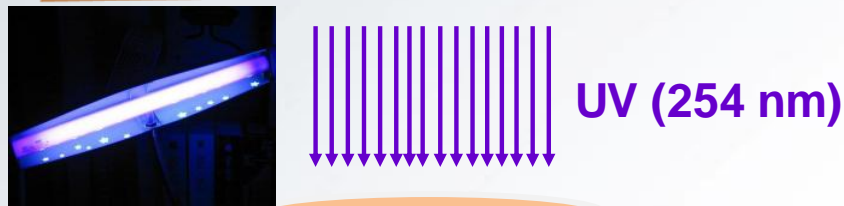
NPs	DLS size in diameter (nm)	TEM Size in diameter (nm)	Results				NPs	DLS size in diameter (nm)	TEM Size in diameter (nm)	Results			
			•OH	¹ O ₂	O ₂ ^{•-}	ROS				•OH	¹ O ₂	O ₂ ^{•-}	ROS
TiO ₂	364					Y	SiO ₂ -NH ₄ OH/NaCl/Na ₃ AlO ₃	13.3,				Y	
	175					N		15.3					
	175					N		590±10					
	826-2368				√			4	15±5				Y
	800-1900								1.6±0.2 (only core)				Y
	79			√	√	√			1.6±0.2 (only core)				Y
	79					√			1.6±0.2 (only core)				Y
				√					1.6±0.2 (only core)				N
CeO ₂	612	15-45				Y	Si- COOH	15, 100		√			
		20±3				N	Ag	5-10				Y	
	2610					Y	Ag- PVA	15				Y	
		6, 12, and 1000				Y	γ-Al ₂ O ₃	15				Y	
		14				Y	α-Al ₂ O ₃	50		√			
ZnO	50-300	20				Y	AuNPs-TPPMS	300		√			
	413				√	Y	AuNPs	1.4				Y	
ZnO/PEG	800					Y		22.1±1.9				Y	
Fe ₂ O ₃	93					Y	Co ₃ O ₄		11.4 (by SSA)			Y	

Almost all types of engineered NPs were reported to produce ROS!

NPs	DLS size in diameter (nm)	TEM Size in diameter (nm)	Results				NPs	DLS size in diameter (nm)	TEM Size in diameter (nm)	Results				
			•O H	¹ O 2	O ₂ ^{•-}	ROS				•O H	¹ O 2	O ₂ ^{•-}	ROS	
Mn ₃ O ₄		12.2 (by SSA)				Y	Polystyrene-COOH	56	<100					N
		12	√					82	<100					N
² O ₃					√		Fullerene	20.5			√			N
CdTe QDs					√									
InP/ZnS QDs		2.8	√		√						√		√	
CdS QDs- mercaptoacetic acid (MPA)		3	√		√		Fullerene-PVP	4.4			√	√		Y
CdSe QDs- MPA)		4.4	√				Fullerene-polymer (polyvinylprrolidone)				√			
CdSe/ZnS QDs- MPA)		4				N	Fullerene-Triton X100; Brij 78;					√	√	
CdSe/ZnS QDs- biotin			√		√		Ozonated C ₆₀				√	√	√	
CdTe QDs - MPA	20				√		Aggregates of C ₆₀	64, 84						N
CdTe QDs- MPA					√			122			√			
Polystyrene-NH ₂	65	<100				N		122			√	√		
Polystyrene-NH ₂	527	<100				Y	fullerol(hydroxylated C ₆₀)	218			√			Y
								106						N

Example 1: Photobleaching or photo-oxidation of QDs, a chemical reaction driven by ROS production

Photochemical Experiments



QDs Solution

• ions • particles

Centrifugal
Separation

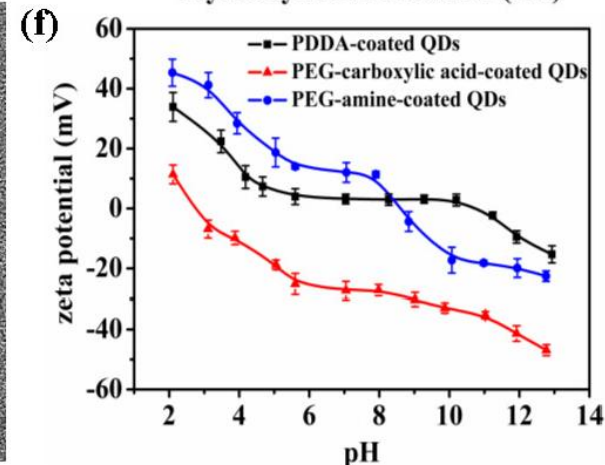
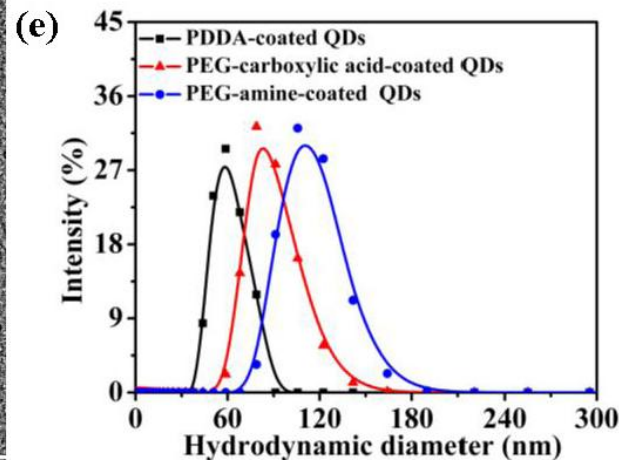
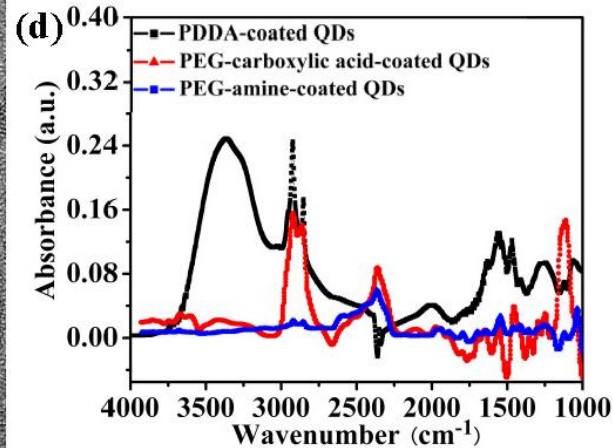
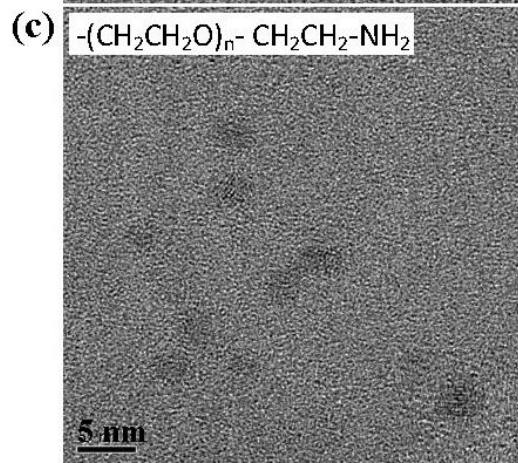
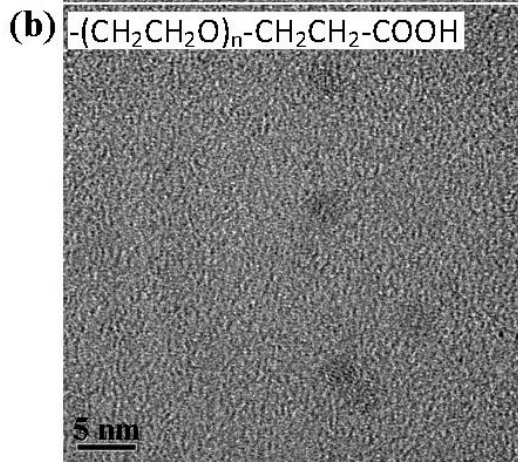
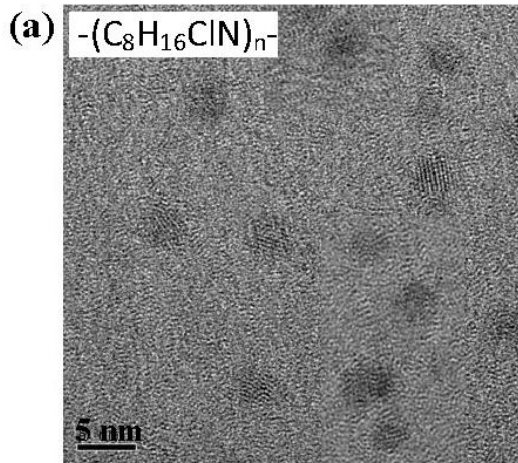
Membrane with
nominal pore
size 1-2 nm



Ion Concentration Measurement with ICP-MS

- Environmental effects (irradiation intensity, temperature, dissolved oxygen, and dissolved organic matter)
- Coating effect

Characterization of QDs



(a)-(c) HR-TEM images of Polydiallyldimethylammounium chloride (PDDA)-, PEG-carboxylic acid-, and PEG-amine-coated QDs, (d) FTIR spectra, (e) Intensity-averaged PSD diagrams, and (f) zeta-potentials as a function of pH for the three types of QDs.

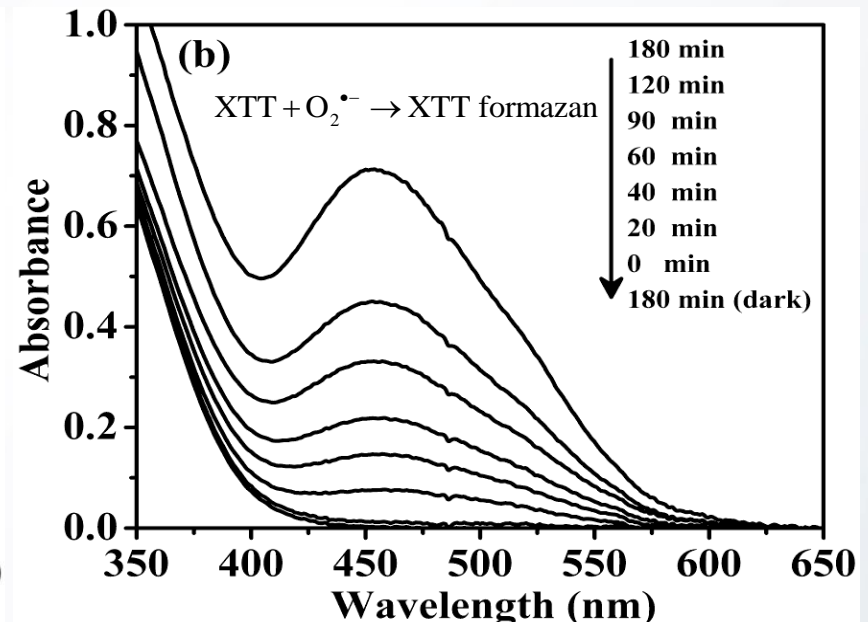
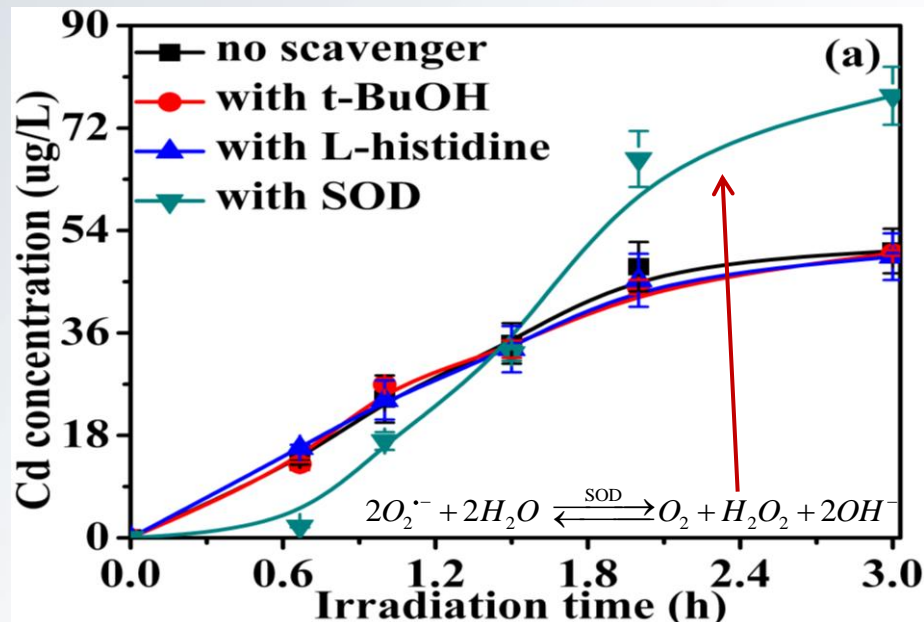
1. CdSe/ZnS as the core
2. 3-5 nm in diameter (TEM)
3. Different surface coating and surface charge

Yang Li, Wen Zhang, Kungang Li, Ying Yao, Junfeng Niu, and Yongsheng Chen. Oxidative dissolution of polymer-encapsulated CdSe/ZnS quantum dots under UV irradiation: mechanisms and kinetics. *Journal of Physical Chemistry C*, Submitted.

Example 1: ROS measurement, an indirect indication using scavengers

Scavenging experiments:

- t-BuOH (30 mM), l-histidine (80 mM) and superoxide dismutase (SOD) (2000 unit/L) from *Escherichia coli* were used to scavenge $\bullet\text{OH}$, $^1\text{O}_2$, and $\text{O}_2^{\bullet-}$, respectively.
- Monitoring the release rates of Cd and Se to indicate the presence of ROS ($\text{O}_2^{\bullet-}$).



(a) Dissolution kinetics of PDDA-coated QDs in the presence and absence of scavengers (initial concentration of QDs $140 \pm 3 \mu\text{g-Cd/L}$, t-BuOH 30 mM, l-histidine 80 mM, and SOD 2,000 unit/L), (b) UV-Vis absorption spectra of PDDA-coated QDs in the presence of XTT as a function of irradiation time (initial concentration of QDs $1.4 \pm 0.03 \text{ mg -Cd/L}$ and XTT 0.15 mM)

Example 2: Another indirect ROS measurement method using indicators

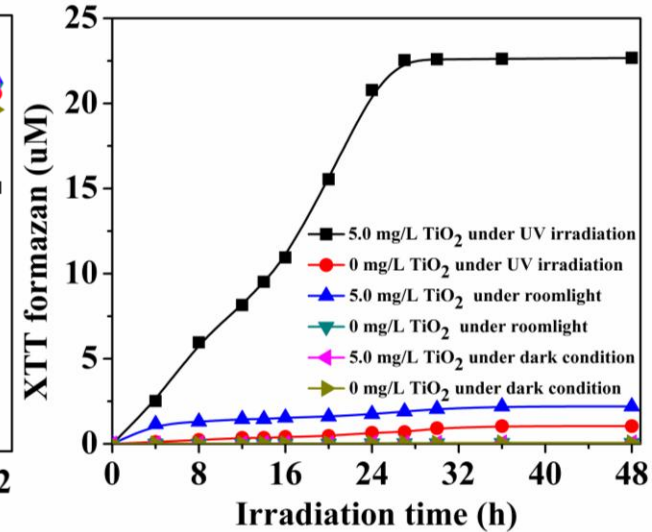
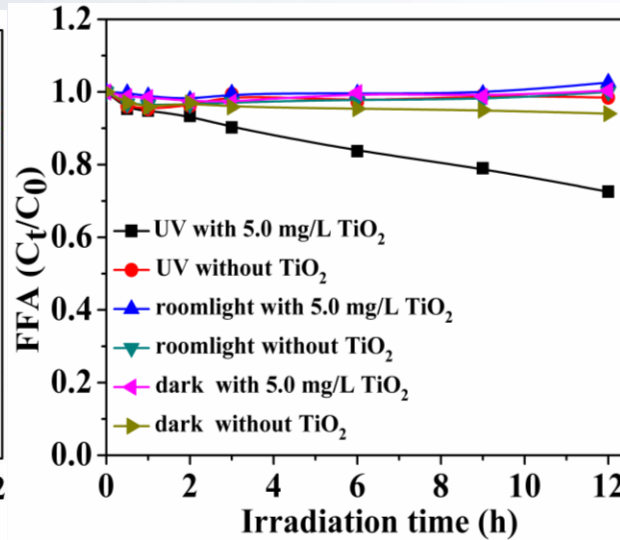
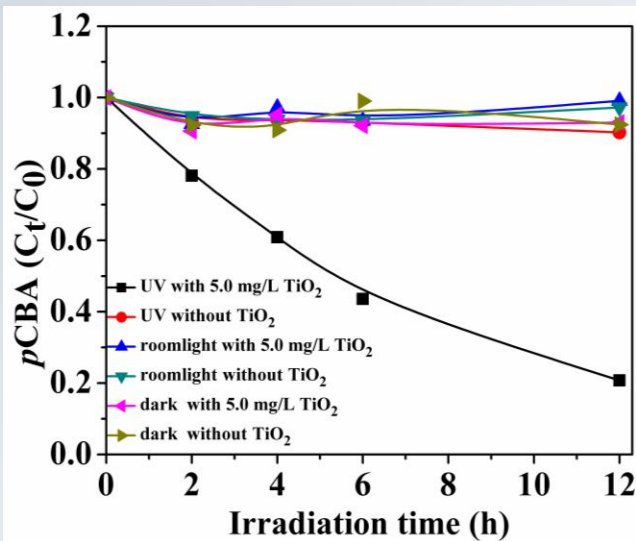
Methods of probing ROS generation from different types of NPs

ROS	$\bullet\text{OH}$	$^1\text{O}_2$	$\text{O}_2^{\bullet-}$
Method	HPLC	HPLC	UV-Vis (430 nm)
Indicator	<i>p</i> CBA	FFA	XTT

Preliminary results

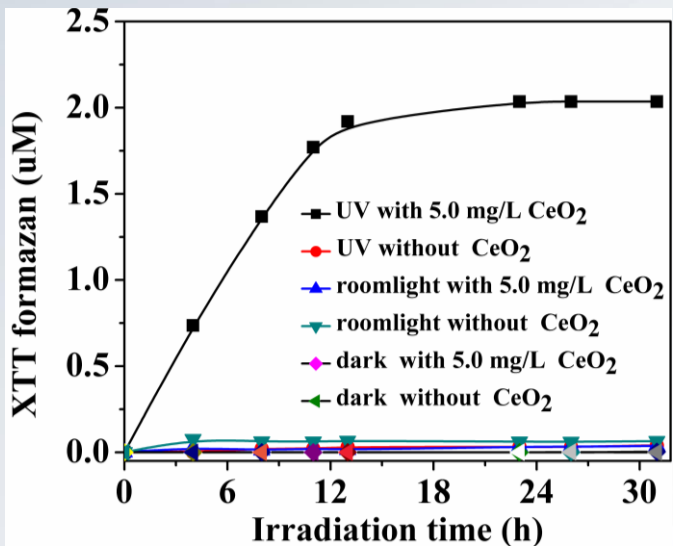
NPs	$\bullet\text{OH}$	$^1\text{O}_2$	$\text{O}_2^{\bullet-}$
TiO ₂	√	√	√
CeO ₂			√
SiO ₂			
ZnO	√		√
CuO	Under investigation		
AuNPs			

ROS generation on different NPs (TiO_2 , CeO_2 , and ZnO as examples)

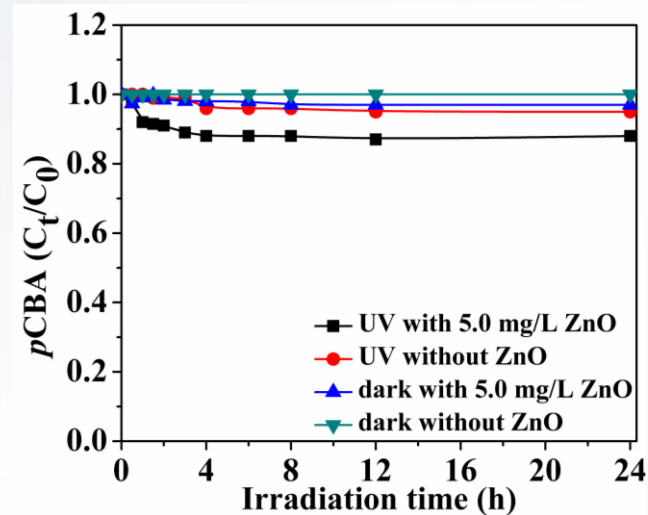


- TiO_2 NPs produces three types of ROS under UV.
- Under room light or dark environment, no significant ROS were detected.

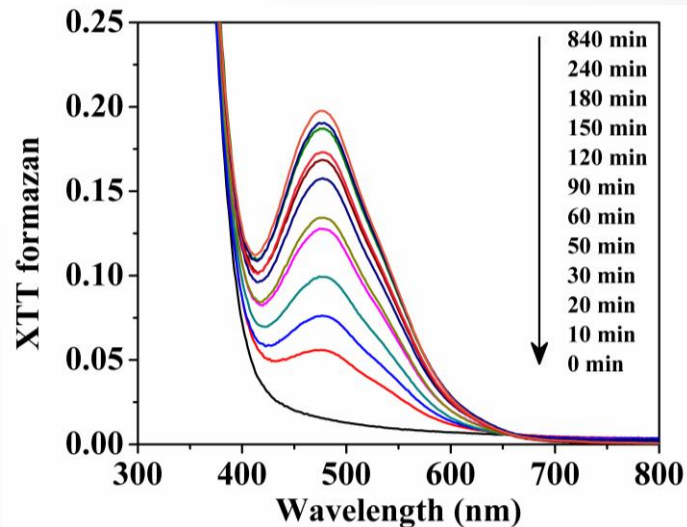
ROS generation on different NPs (TiO₂, CeO₂, and ZnO as examples)



➤ CeO₂ NPs were found to produce O₂^{•-} only.



➤ ZnO NPs produced •OH and O₂^{•-}



Quantitative relationship between ROS production and toxic potential (ongoing research)

Now, I propose to assign the weight factors and calculate the “ROS index” for each type of NPs that is further used to draw a relationship with mortality rates (as an indicator of toxic potential).

Different ROS/NPs	$\bullet\text{OH}$	$^1\text{O}_2$	$\text{O}_2^{\bullet-}$
Weight	A1	A2	A3
ROS production rate constant (s^{-1})	k1	k2	k3
ROS index=	$A1 \cdot k1 + A2 \cdot k2 + A3 \cdot k3$		

Take-home messages

- Physical and chemical insight into nanotoxicity.
- Changes in biomechanical and electrical properties may interpret the surface disruption
- ROS leads to the chemical irritation for cells and is widely detected in many types of engineered NPs.

Acknowledgements

Advisor: Dr. Yongsheng Chen

PhD student:

Kungang Li, Jia Yang, Wei Zhang,
Jin Gi Hong

Research scientist:

Wen Zhang

Exchange student:

Yang Li

Visiting scholar:

Ying Chen

Funding agency:

- **U.S. Environmental Protection Agency Science to Achieve Results Program Grant RD-83385601;**
- **Semiconductor Research Corporation (SRC)/ESH grant (425.025).**

